Global and Planetary Change 195 (2020) 103361

Contents lists available at ScienceDirect

Global and Planetary Change

journal homepage: www.elsevier.com/locate/gloplacha

Understanding partitioning of deformation in highly arcuate orogenic systems: Inferences from the evolution of the Serbian Carpathians

Nemanja Krstekanić [a,b,*], Liviu Matenco [a], Marinko Toljić [b], Oleg Mandic [c], Uros Stojadinovic [b], Ernst Willingshofer [a]

[a] Utrecht University, Faculty of Geosciences, Utrecht, The Netherlands
[b] University of Belgrade, Faculty of Mining and Geology, Belgrade, Serbia
[c] Natural History Museum Vienna, Geological-Paleontological Department, Austria

ARTICLE INFO

Keywords:
Orogenic building
Oroclines
Multi-directional extension
Strike-slip
Serbian Carpathians

ABSTRACT

Highly curved orogens often demonstrate a complex poly-phase tectonic evolution and significant strain partitioning. While the oroclinal bending towards the outer arc is understood to be often driven by rapid slab roll-back, processes driving such bending towards the back-arc domain are less understood. The Serbian segment of the larger, highly bended Carpathians–Balkanides Mountains is one key example where we studied the kinematics of nappe stacking and the mechanics of oroclinal bending by the means of a field kinematic study correlated with available information in adjacent orogenic segments. Although not apparent in the large-scale structure of the Serbian Carpathians, our results demonstrate a poly-phase evolution, where the late Early Cretaceous nappe stacking was followed by Oligocene–middle Miocene ~40° of clockwise rotations. The superposition of Dinarides extension with the oroclinal bending in the Carpathians created overlapping stages of orogen-perpendicular extension and dextral strike-slip coupled with orogen-parallel extension, driven by the 100 km cumulated offset of the Cerna and Timok Faults. Extension was associated with the formation of Oligocene–Miocene basins, providing critical timing constraints for our kinematic study. These deformations were followed by the late Miocene *E*-ward thrusting of the Upper Getic sub-unit, which was driven by a transfer of deformation in the orocline and around the Moesian Platform during the last stages of Carpathians collision. These results show that the mechanics of oroclinal bending is associated with the activation of strike-slip faults and strain partitioning by bi-modal extension, enhanced by the overlap between different geodynamic processes.

1. Introduction

The formation of highly arcuate orogenic systems has been documented in numerous worldwide studies, such as in the Altai and Alborz Mountains, New England Orogen, Dun Mountain Ophiolite Belt, South Andes, Ouachita Orogen, or the various mountain chains composing the Mediterranean area (e.g., Calignano et al., 2017; Edel et al., 2014; Li and Rosenbaum, 2014; Lonergan and White, 1997; Mattei et al., 2017; Meijers et al., 2010; Mortimer, 2014; Pastor-Galán et al., 2015; Rosenbaum, 2012, 2014; Torres Carbonell et al., 2016; Vergés and Fernàndez, 2012; Xiao et al., 2018). These studies have demonstrated that the formation of highly arcuate orogenic systems may be related to a number of processes influenced by inherited rheological heterogeneities, such as the variability of deformation in orogens influenced by slab roll-back or slab tearing mechanics, lithospheric folding or lateral variations in the geometry of plate boundaries and rigid indenters (e.g., Calignano et al., 2017; Hollingsworth et al., 2010; Pastor-Galán et al., 2012; Rosenbaum, 2014; Zweigel et al., 1998 and references therein). These highly curved orogens are sometimes referred as oroclines, which acquired their curvature during and/or after the main orogenic process, or by subsequent bending of a primary arc (e.g., Carey, 1955; Cifelli et al., 2008; D'el-Rey Silva et al., 2011; Johnston et al., 2013; Platt et al., 2003; Rosenbaum, 2014). The term strain partitioning has been used in many different ways at different spatial scales (e.g., Carreras et al., 2013; Lister and Williams, 1983), from large strike-slip faults parallel to subduction zones accommodating oblique convergence (e.g., Fitch, 1972; Platt, 1993), coeval pure-shear and simple-shear strain that accommodate zone-perpendicular and zone-parallel deformation, respectively (Fossen et al., 1994; Jones and Tanner, 1995), or a multi-scale distribution of bulk strain to different genetic types of coeval structures that

* Corresponding author at: Utrecht University, Faculty of Geosciences, Utrecht, The Netherlands.
E-mail address: n.krstekanic@uu.nl (N. Krstekanić).

https://doi.org/10.1016/j.gloplacha.2020.103361
Received 16 March 2020; Received in revised form 11 September 2020; Accepted 19 October 2020
Available online 27 October 2020

cannot be defined by a uniform stress field (e.g., Benesh et al., 2014; Cembrano et al., 2005; D'el-Rey Silva et al., 2011; De Vicente et al., 2009; Glen, 2004; Krézsek et al., 2013). We adopt the latter, more general meaning of strain partitioning to describe coeval structures of different genetic type associated with oroclinal bending.

In all situations, oroclinal bending is associated with large amounts of strain partitioning in various segments of the orocline, which makes it difficult to use standard field kinematic approaches based on the consistency of strain or paleostress directions along the orogenic strike (e.g., D'el-Rey Silva et al., 2011; Glen, 2004; Lacombe, 2012; Li et al., 2018; Pastor-Galán et al., 2011; Ries and Shackleton, 1976). Oroclinal bending towards the outer arc (the convex side oriented towards towards the foreland, i.e. herewith defined foreland-convex) displays significant strain partitioning during orogenic thrusting and backarc extension, being driven often by slab retreat, as commonly observed in the Apennines, Betics–Rif, Hellenides or Carpathians orogens of the Mediterranean system (Fig. 1a, e.g., Faccenna et al., 2004; Jolivet et al., 2013). The formation of such oroclines is also associated with orogen-parallel extension and the evolution of large-scale strike-slip systems (e.g., Gutiérrez-Alonso et al., 2015; Martínez-García et al., 2013; Roldán et al., 2014), which potentially compete with backarc, orogen-perpendicular extension driven by slab retreat and coeval shortening mechanics (e.g., Faccenna et al., 2014; Menant et al., 2016a, 2016b). However, the interplay between these processes is less understood due to their genetic separation in different locations across the strike of the orogen and the complexity of kinematics in oroclinal bending. This lack of knowledge is particularly valid in places where oroclinal bending takes place towards the backarc (Fig. 1a, the convex side towards the backarc, i.e. herewith defined backarc-convex).

One of the best examples of oroclinal bending in Mediterranean orogens is the double 180° arcuate loop of the Carpathians–Balkanides orogenic system. While the foreland-convex orocline segment composed of the West, East and South Carpathians formed in direct response to the Paleogene–Miocene slab retreat, the backarc-convex orocline segment composed of the Balkanides, Serbian and South Carpathians formed during coeval rotations and docking against the Moesian Platform (Fig. 1; e.g., Maţenco, 2017; Ratschbacher et al., 1993). The formation of this exceptional orocline was associated with opposite sense rotations of the two main continental blocks that make up the upper tectonic plate (i.e., ALCAPA and Tisza–Dacia mega-unit; Fig. 1a) during the gradual Cretaceous–Miocene closure of the external Carpathians embayment by subduction and collision (e.g., Csontos and Vörös, 2004; Horváth et al., 2015). The Cretaceous formation of the Carpathian thick-skinned nappe stack was followed by a gradual clockwise rotation and N-, N*E*- to E-ward translation of the Tisza–Dacia mega-unit (e.g., Balla, 1987; Csontos, 1995; Márton, 2000; Pătraşcu et al., 1994; Panaiotu and Panaiotu, 2010; Ustaszewski et al., 2008). In respect to the stable European units situated in the foreland of the Carpathians, this Tisza–Dacia mega-unit underwent up to 90° of clockwise rotations during post-Cretaceous times (Pătraşcu et al., 1990, 1992, 1993; Panaiotu and Panaiotu, 2010), of which 15°-30° was achieved during post-middle Miocene times (de Leeuw et al., 2013; Dupont-Nivet et al., 2005). The amount of clockwise rotation decreases southwards to no significant rotations in the Balkanides during the Cenozoic (van Hinsbergen et al., 2008). In the studied segment of the Serbian Carpathians, available paleomagnetic data suggest only ~25° clockwise rotation during post-Cretaceous times (Lesić et al., 2019 and references therein), while structural interpretations have inferred 10° clockwise rotation during post-Oligocene times (Marović et al., 2002). The neighbouring segment of the Dinarides orogen recorded 34°-46° clockwise rotations during post-early Miocene times (Lesić et al. (2019).

These rotations and translations were associated with Eocene–early Miocene orogen-parallel extension and ~ 100 km of dextral strike-slip offset along the curved Cerna–Jiu and Timok faults system in the South and Serbian Carpathians, and a gradual transtensive opening of basins in their foreland, which was accommodated by coeval shortening in the East Carpathians (Fig. 1b; Fügenschuh and Schmid, 2005; Krézsek et al., 2013; Matenco and Schmid, 1999; Schmid et al., 1998). All these large-scale movements were partly coeval with the Oligocene–Miocene orogen perpendicular back-arc extension recorded by the Tisza–Dacia part of the larger Pannonian Basin and its southern prolongation along the Morava Valley Corridor (e.g., Figs. 1b, 2; Balázs et al., 2016; Erak et al., 2017; Horváth et al., 2006; Toljić et al., 2013). This prolongation presently separates the orogenic structure of the Dinarides from the one of the Carpathians (Fig. 1b). The Pannonian Basin extension was followed by an overall N- to NE- ward indentation of the Adriatic continental microplate that inverted the southern part of the Pannonian Basin starting with the latest Miocene (e.g., Matenco and Radivojević, 2012; Pinter et al., 2005). This overall evolution infers the juxtaposition of orogen-perpendicular extension, orogen-parallel extension and strike-slip deformation in the area of the Morava Valley Corridor and the adjacent N-S oriented segment of the Serbian Carpathians (Figs. 1 and 2; e.g., Erak et al., 2017). Furthermore, this is the same area where orogenic extension driven by eduction or roll-back in the Dinarides system has been inferred (Andrić et al., 2018; Matenco and Radivojević, 2012). In this overall framework, the evolution of the Serbian Carpathians segment is still less constrained, although available structural and paleomagnetic studies indicate that its oroclinal bending connected with the Balkanides and the South Carpathians was largely achieved during the Oligocene–Miocene (e.g., Csontos et al., 1992; Márton, 2000; Márton et al., 2007; de Leeuw et al., 2013). More recent regional paleostress reconstructions indicate a stress field with variable orientations that formed during the gradual clockwise rotation around the Moesian Platform (Mladenović et al., 2019). However, how such a variable stress field is linked with the mechanics of regional and local deformation during the clockwise Carpathians rotation and the formation of extensional intra-montane and back-arc basins remains unclear.

We aim to understand the relationship between nappe stacking, orogen-perpendicular and orogen-parallel extension associated with strike-slip deformation during the backarc-convex oroclinal bending of the Carpathians–Balkanides Mountains. To this aim, we have performed a kinematic field study in the internal part of the Serbian Carpathians near their contact with the Dinarides, which is the key area of interference between the orogen-parallel and orogen-perpendicular extension. Our study is correlated with the evolution of Oligocene - Miocene basins, together with orogenic nappe stacking kinematic and timing constraints available in more external areas of the Serbian Carpathians and the neighbouring areas of the Dinarides, Morava Valley Corridor, South Carpathians and Balkanides (Fig. 1). The results are discussed in the context of the regional evolution of Carpathians–Balkanides and Dinarides orogenic systems and in terms of strain partitioning during oroclinal bending.

2. Tectonic evolution of the Serbian Carpathians and associated sedimentary basins

The Serbian segment of the Carpathians–Balkanides forms part of the larger Europe-derived Dacia tectonic mega-unit (Fig. 1b). This segment is located in the area of interference between the nappe stacking recorded by two orogenic systems that formed during the closure of two oceanic realms, i.e. the Ceahlău–Severin branch of the Alpine Tethys Ocean and a northern branch of the Neotethys Ocean (e.g., Schmid et al., 2008, 2020).

2.1. The Cretaceous–Eocene tectono-stratigraphy and associated magmatism

The Ceahlău–Severin branch of the Alpine Tethys Ocean, whose remnants outcrop east and north of the studied area (Figs. 1 and 2), opened during the Middle Jurassic and was closed by Cretaceous subduction and collision, while its remnants were further deformed during Late Cretaceous–Miocene times (e.g., Maţenco, 2017; Schmid et al.,

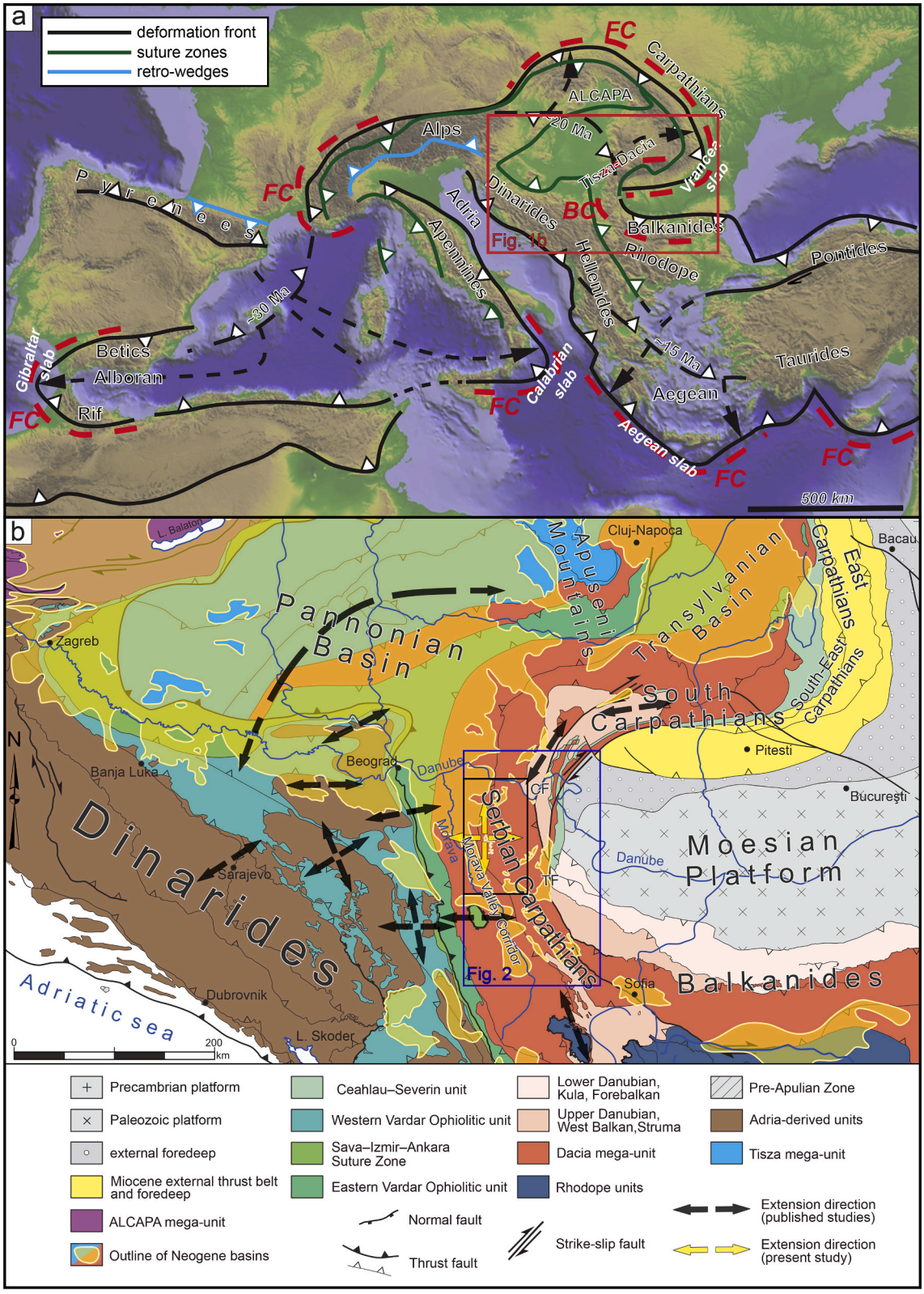

Fig. 1. a) Simplified image of Mediterranean orogens formed during Mesozoic - Cenozoic times, displaying suture zones, orogenic fronts and retro-wedges (inspired from van Hinsbergen et al., 2020). Dashed red lines are oroclines. FC = foreland-convex orocline; BC - backarc-convex orocline; Red rectangle shows the location of Fig. 1b. b) Regional tectonic map of the area connecting the Dinarides and South Carpathians showing the main tectonic units (modified after Schmid et al., 2008, 2020). Blue rectangle shows the location of Fig. 2, the black rectangle indicates the locations of Figs. 5, 7, 8 and 10. Extension directions are plotted after Andrić et al. (2017), Erak et al. (2017), Fügenschuh and Schmid (2005), Kounov et al. (2011), Matenco and Radivojević (2012), Mladenović et al. (2015), Porkoláb et al. (2019); Schefer (2012), Stojadinovic et al. (2013, 2017) and Toljić et al. (2013). TF-Timok Fault; CF-Cerna Fault. (For interpretation of the references to colour in this figure legend, the reader is referred to the web version of this article.)

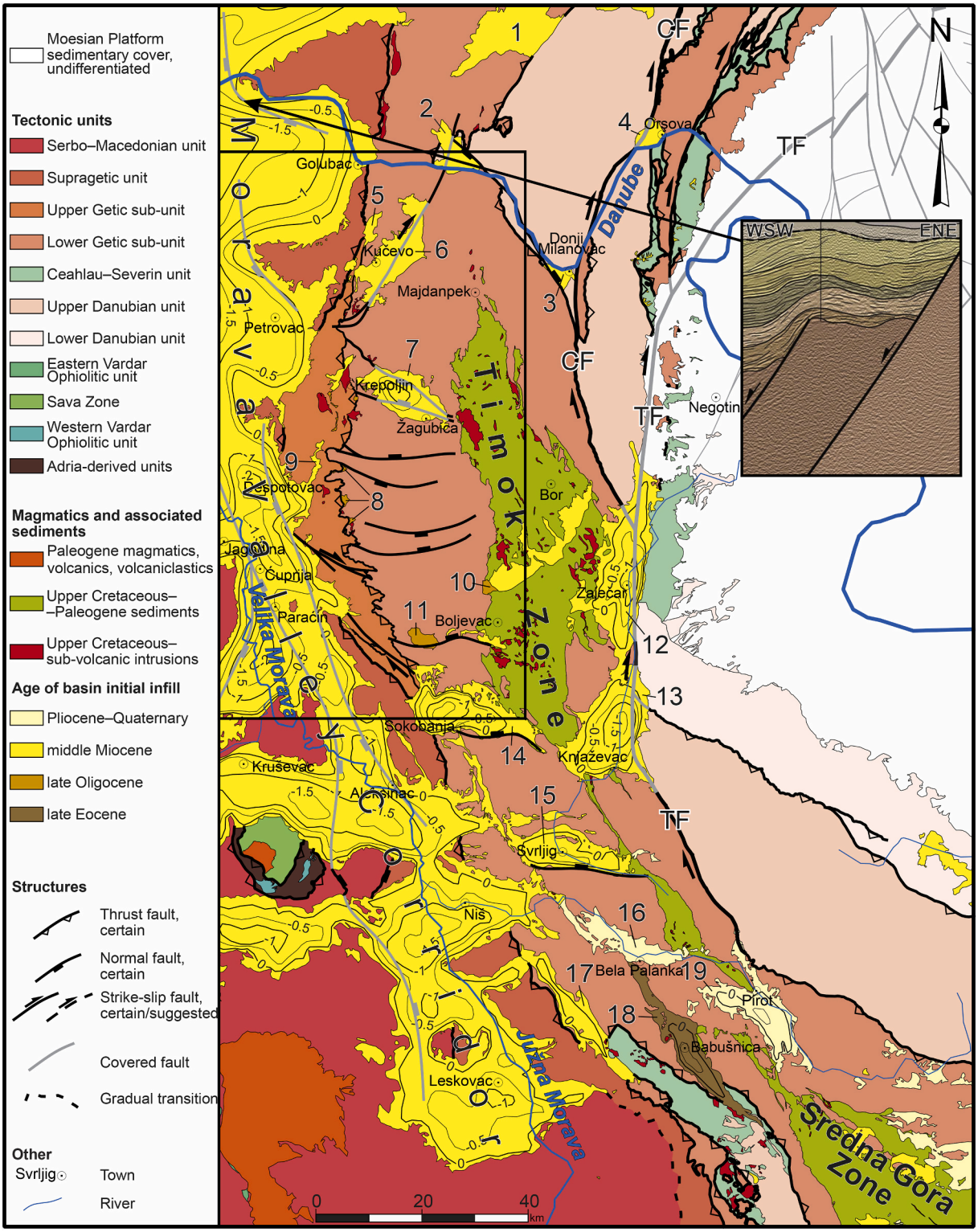

Fig. 2. Tectonic map of the Serbian Carpathians and adjacent areas of the South Carpathians and Balkanides showing the regional fault kinematics (compiled and modified after Basic geological map of former Yugoslavia, scale 1:100.000 and Maţenco, 2017). Isolines in Cenozoic basins indicate pre-Cenozoic basement structure (compiled after Balázs et al., 2016 and Matenco and Radivojević, 2012). Isoline numbers are in kilometres. Black rectangle indicates the position of Figs. 5, 7, 8 and 10. TF-Timok Fault; CF-Cerna Fault. Intramontane basins: 1-Bozovici Basin, 2-Sichevița Basin, 3-Donji Milanovac Basin, 4-Orşova Basin, 5-Rakova Bara Basin, 6-Kučevo Basin, 7-Žagubica Basin, 8-Senje–Resava Basin, 9-Panjevac Basin, 10-Bogovina Basin, 11-Krivi Vir Basin, 12-Timok Basin, 13-Knjaževac Basin, 14-Sokobanja Basin, 15-Svrljig Basin, 16-Bela Palanka Basin, 17-Zaplanje Basin, 18-Babušnica Basin, 19-Pirot Basin. Inset: Segment of a seismic cross-section of Matenco and Radivojević (2012), showing *syn*-sedimentary faults in the Morava Valley Corridor.

2008). To the east, the stable European foreland is made up by the Moesian Platform in the area adjacent to the South and Serbian Carpathians (Fig. 1, Săndulescu, 1988; Visarion et al., 1988). In this segment of the orogen, the Cretaceous closure by subduction and subsequent collision of the Ceahlău–Severin Ocean was associated with two main stages of shortening that created the presently observed nappe stack. The initial late Early Cretaceous thrusting (~100–110 Ma, 'Austrian' event in local literature) of the Supragetic unit was followed by the latest Cretaceous thrusting (late Campanian–early Maastrichtian, ~75–67 Ma, 'Laramian' event in local literature) of the Getic unit and the formation

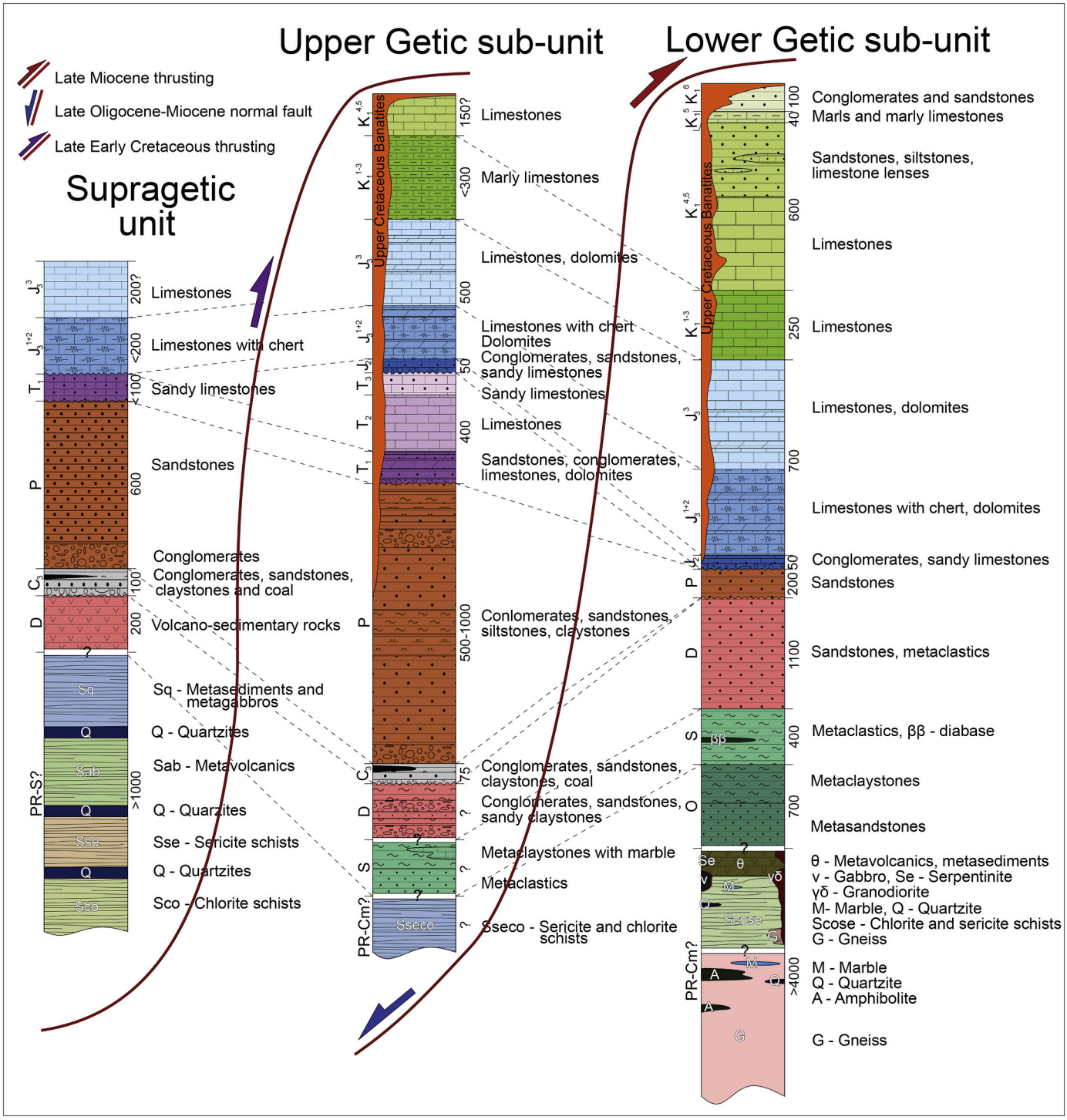

Fig. 3. Tectono-stratigraphic columns of Supragetic, Upper Getic and Lower Getic sub-units in the studied area (compiled and correlated after Basic geological map of former Yugoslavia, scale 1:100.000). Purple half arrow indicates the late Early Cretaceous shortening and nappe-stacking that created the Supragetic thrust, while blue and red half arrows illustrates Miocene normal faulting and thrusting, respectively, of the Upper Getic thrust. Stratigraphic age of the units is indicated by the symbols on the left side of each column (PR-Proterozoic; Cm-Cambrian; O-Ordovician; S-Silurian; D-Devonian; C_3-Upper Carboniferous; P-Permian; T_1-Lower Triassic; T_2-Middle Triassic; T_3-Upper Triassic; J_2-Middle Jurassic; J_3^{1+2}-Oxfordian-Kimmeridgian; J_3^3-Tithonian; K_1^{1-3}-Berriasian-Hauterivian; $K_1^{4,5}$-Barremian-Aptian; K_1^5-Aptian; K_1^6-Albian). Numbers on the right side of each column represent the maximal thickness of units in meters. (For interpretation of the references to colour in this figure legend, the reader is referred to the web version of this article.)

of a Danubian nappe stack derived from the margin of the Moesian Platform (e.g., Csontos and Vörös, 2004; Iancu et al., 2005a; Neubauer, 2015; Săndulescu, 1988; Seghedi et al., 2005). These events were coeval with significant exhumation of the entire nappe stack, well quantified by thermochronological studies in the South Carpathians (e.g., Bojar et al., 1998; Fügenschuh and Schmid, 2005; Neubauer and Bojar, 2013; Willingshofer et al., 1999).

The Supragetic unit exposes a metamorphic basement made up of a Neoproterozoic–Silurian volcano-sedimentary sequence metamorphosed dominantly in greenschist to sub-greenschist facies in the

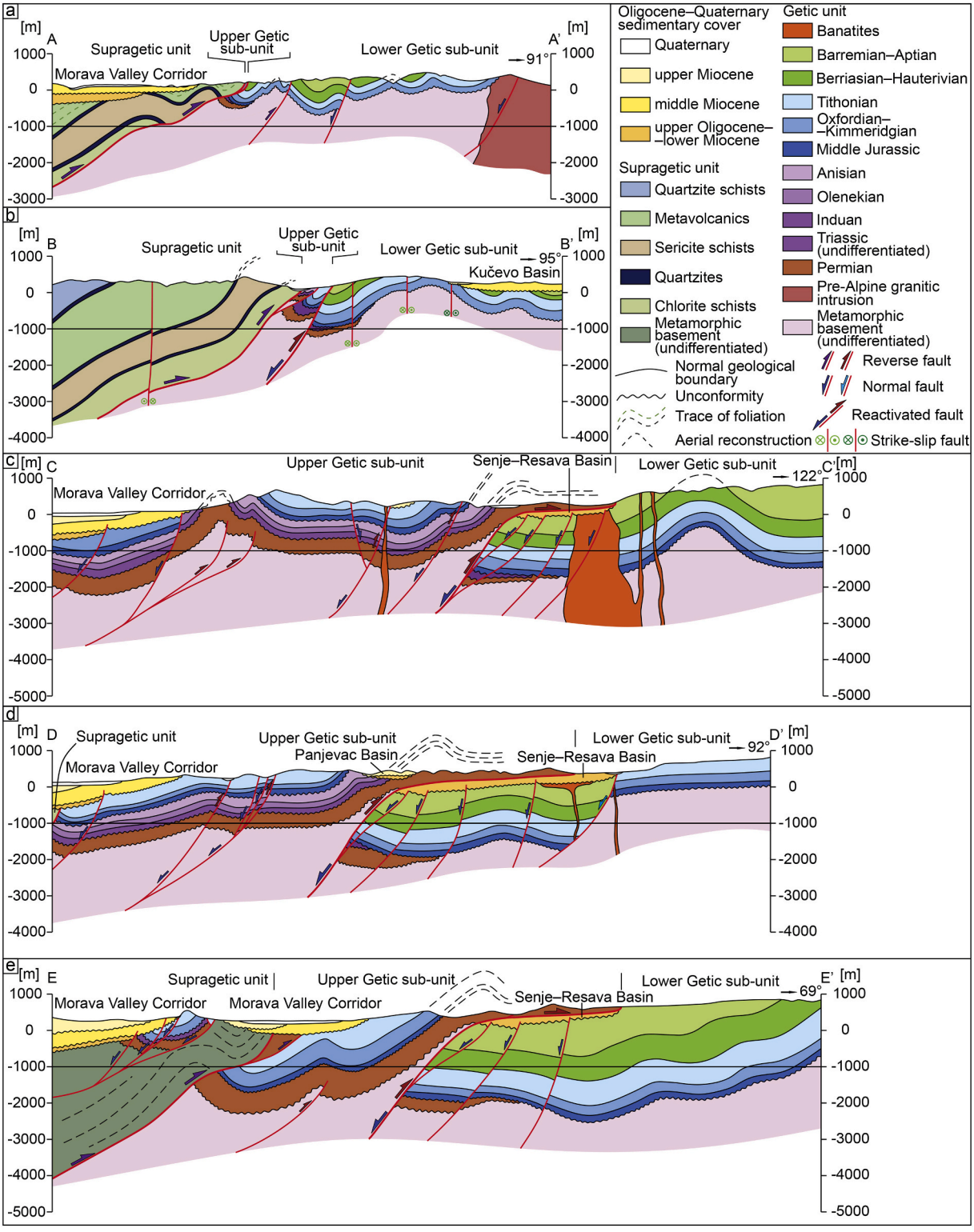

Fig. 4. Geological cross sections across the studied area. Cross sections are built following the field observations and results of this study. Surface to depth projection is based on the field kinematic data from this study and the Basic geological map of former Yugoslavia, scale 1:100.000. Colors of half-arrows indicating kinematics along faults are same as respective structures in Figs. 5, 7 and 10. Sections a) and b) are modified after Krstekanić et al. (2017). The positions of the cross sections are displayed in Figs. 5, 7, 8 and 10. The strike of each cross section is indicated in the upper right corner of the section. No vertical exaggeration.

Serbian Carpathians and amphibolite to sub-greenschist facies in the South Carpathians during Variscan times (Figs. 3, 4; Iancu et al., 2005b; Kalenić et al., 1980). In the Serbian Carpathians, these rocks are overlain by a transgressive-regressive upper Carboniferous–Permian sequence containing conglomerates, sandstones and shales with coal seams that are replaced upwards in the stratigraphy by red alluvial sandstones (Fig. 3, Djordjević-Milutinović, 2010; Kalenić et al., 1980; Petković, 1975). These sediments are overlain by a transgressive Triassic–Jurassic alluvial to shallow-water limestone sequence (Veselinović et al., 1970). The Getic unit is separated in the Serbian Carpathians in two sub-units (the Upper and Lower Getic, Figs. 2, 4) by a large-offset thrust (Figs. 2, 4). Northwards, the late Early Cretaceous thrusting has created in the South Carpathians a narrow system of two nappes located in the upper part of the Getic unit that contain Triassic–Jurassic sediments and are found immediately beneath the main Supragetic thrust (the Sasca–Gornjac and Resita nappes, Iancu et al., 2005a). These nappes were interpreted to be the equivalent of the Upper Getic sub-unit emplaced during late Early Cretaceous times in a trailing imbricated fan sequence in the footwall of the main Supragetic thrust (e.g., Kräutner and Krstić, 2002; Săndulescu, 1984). The Upper and Lower Getic sub-units contain a similar Variscan greenschist to amphibolite facies metamorphosed basement that is intruded by plutons and overlain by an Upper Carboniferous to Cretaceous sedimentary cover (Figs. 3, 4; Iancu et al., 2005a, 2005b; Kräutner and Krstić, 2003). The Mesozoic cover reaches 2 km in thickness and is composed of a Permian - Lower Triassic transgressive alluvial clastic to shallow-water sequence (Fig. 3) that crops out on a larger area in the Lower Getic sub-unit, unconformably overlain by a sequence containing a mixed Middle Jurassic clastic-carbonatic sequence, Upper Jurassic - Lower Cretaceous shallow-water limestones and dolomites, including a typical Urgonian reef facies, and Aptian–Cenomanian clastics (Fig. 3).

To the west and south of our studied area, the remnants of another ocean crop out, i.e. the northern branch of the Neotethys Ocean (or the Vardar Ocean, Fig. 1b). This ocean opened during Middle Triassic times by separating the European from Adria-derived units, the latter being derived from the larger African domain (e.g., Pamić, 1984; Schmid et al., 2008; Stampfli and Borel, 2002). The Middle Jurassic onset of oceanic subduction led initially to obduction of ophiolites and genetically associated ophiolitic melanges over both the Adriatic- and European-derived continental margins (the Western and Eastern Vardar Ophiolitic units, respectively; Fig. 1b; Dimitrijević, 1997; Schmid et al., 2008). This obduction was followed by Cretaceous–Eocene shortening that peaked during the latest Cretaceous onset of collision and the subsequent formation of a suture zone at the contact between the two main continental units (i.e. the Sava Suture Zone; Pamić, 2002; Stojadinovic et al., 2017; Ustaszewski et al., 2009). The Late Cretaceous subduction of the Neotethys ocean was associated with the emplacement of large volume of magmatism (~92–67 Ma) that is observed in the Apuseni–Banat–Timok–Sredna Gora Zone (ABTS) belt (e.g., Gallhofer et al., 2015; von Quadt et al., 2005). Alternatively, the emplacement of the ABTS magmatic belt has also been interpreted to be driven by subduction of the Ceahlau-Severin Ocean (Neubauer, 2015). East of the studied area in the Timok Zone (Fig. 2) and further to the SE in the Sredna Gora unit, this typical arc calc-alkaline magmas were emplaced as magmatic intrusions, volcanic lava flows and a volcanoclastic sequence in a number of extensional structures that started at ~92–87 Ma, whereas the magmatism becomes progressively younger towards the hinterland (e.g., Gallhofer et al., 2015; Kolb et al., 2013). The onset of this extension was coeval with the formation of an extensional fore-arc basin overlying the European margin adjacent to the Sava Zone (Toljić et al., 2018). This Late Cretaceous extension has also possibly exhumed the high-grade metamorphosed Serbo–Macedonian unit from below the low-grade metamorphosed Supragetic unit along an extensional detachment (Antić et al., 2016a; Erak et al., 2017). However, the exact nature of this reactivated Paleozoic (Caledonian and Variscan) Serbo–Macedonian\Supragetic contact is poorly known, owing to its often burial beneath the Paleogene–Neogene sediments along the Morava Valley Corridor (Fig. 2; Antić et al., 2016b; Săndulescu, 1984). Other magmatic intrusions and volcanics are observed W to SSW of the studied area in three roughly parallel belts, emplaced during latest Cretaceous, Eocene–Oligocene and Miocene times, which are thought to be related with an overall SW-ward migration and detachment of the Neotethys slab (Andrić et al., 2018 and references therein).

2.2. *The Eocene–Miocene orogen-parallel and perpendicular extension associated with large scale transcurrent motions*

The study area lies in the transition zone between orogen parallel and perpendicular extensions and strike-slip deformation that took place during the clockwise rotation of the Carpathians units (Fig. 1). In more details, an orogen-parallel extensional detachment formed during Paleocene–Eocene times in the South Carpathians by the reactivation of the inherited Getic unit thrust contact and the exhumation of Danubian nappe stack in its footwall (e.g., Fügenschuh and Schmid, 2005; Matenco and Schmid, 1999; Moser et al., 2005; Schmid et al., 1998). This orogen-parallel deformation continued by the activation of the late Oligocene Cerna and the early Miocene Timok faults system that retained 35 and 65 km offsets, respectively, in the South and Serbian Carpathians (Berza and Drăgănescu, 1988; Kräutner and Krstić, 2002). The activity along these strike-slip faults is partly coeval with the second, Miocene cooling event that was associated with a low magnitude of vertical movements (Moser et al., 2005). The onset of an *E*-W oriented extension (i.e. orogen-perpendicular for the study area) took place in or near the Morava Valley Corridor (Figs. 1 and 2) during Oligocene times (~29–27 Ma, based on thermochronological data of Erak et al., 2017), while the same basin was subsequently enlarged during the peak moments of extension that took place during the middle Miocene (~15–13 Ma), creating the well observed *syn*-kinematic deposition (e.g., inset in Fig. 2, see also Matenco and Radivojević, 2012; Stojadinovic et al., 2013, 2017; Toljić et al., 2013). Large-offset early-middle Miocene normal faults and detachments accommodating a N-S to ENE-WSW oriented extension are observed in the neighbouring Dinarides (e.g., Andrić et al., 2017; Mladenović et al., 2015; Schefer, 2012; Ustaszewski et al., 2010). These structures and genetically associated basins were inverted starting with the latest Miocene, commonly interpreted to be driven by the indentation of the Adriatic microplate, which is still presently active (e.g., Andrić et al., 2017; Bada et al., 2007; Fodor et al., 2005).

The Oligocene - Miocene extension and strike-slip was associated with the formation of a significant number of extensional basins (Fig. 2). In the Morava Valley Corridor, the Oligocene–early Miocene normal faults and *syn*-kinematic sedimentation are usually buried at depth beneath the largely outcropping post-kinematic deposition younger than 17 Ma (Fig. 2, Krstić et al., 2003; Matenco and Radivojević, 2012; Sant et al., 2018). Most of these post-kinematic shallow-water sediments are lacustrine and were deposited dominantly during and after the late Miocene endemic isolation of the Pannonian Basin (e.g., Kalenić et al., 1980; ter Borgh et al., 2013; Vujisić et al., 1981). The intra-montane basins of the Serbian Carpathians (Fig. 2) contain a similar lacustrine facies that has a significant age variability. The oldest sediments are the middle to upper Eocene lacustrine turbidites observed at the base of the Babušnica Basin (de Bruijn et al., 2018; Marković et al., 2017). The late Oligocene–early Miocene Senje–Resava and Bogovina basins (including the Panjevac and Krivi Vir sub-basins, Fig. 2, Lihoreau et al., 2004; Mai, 1995; Maksimović, 1956; Obradović and Vasić, 2007; Pavlović, 1997; Žujović, 1886) are thrusted by Permian sandstones of the Upper Getic sub-unit (Fig. 4). Most of other basins have an early middle Miocene initial infill, while being overlain by late Miocene–Pliocene sedimentation, such as the Sokobanja, Žagubica and Svrljig basins (Fig. 2; Kalenić et al., 1980; Lazarević and Milivojević, 2010; Marković, 2003; Obradović and Vasić, 2007; Sant et al., 2018). The sedimentation in the remaining basins (Bela Palanka and Pirot Basins, Fig. 2) is thought to

have started only during Pliocene times (Anđelković et al., 1977; Vujisić et al., 1980).

3. Field structural observations and kinematic analysis

We have performed our fieldwork in the key area of interference between strike-slip, orogen-parallel and orogen-perpendicular extension, which is where the Supragetic and Getic units are in close proximity to the Morava Valley Corridor (Fig. 2). This area benefits from the high quality and full coverage of 1:100.000 scale geological maps (OGK former Yugoslavia). These maps were extensively used previously to define the timing and geometry of the Jurassic - Paleogene deformation by using the observed stratigraphic juxtaposition across faults combined with their overlying post-kinematic sedimentation (e.g., Dimitrijević, 1997; Schmid et al., 2008, 2020 and references therein).

We specifically focused the kinematic fieldwork to characterize the kinematics of large faults and shear zones, initially identified to have large stratigraphic offset (vertical and/or horizontal) in geological maps, such as the thrust of the Supragetic and Upper Getic (sub-)units, large offset normal or strike-slip faults. We confirmed or re-interpreted these structures by measuring their kinematics and large offsets (from hundreds of metres to 20 km) along their strike across the entire studied area (colored faults in Figs. 5, 7, 8 and 10). In the field, these major contacts are observed in the field by zones of intense deformation, such as meters-thick foliated fault gouges, intense faulting with large offset at outcrop scale, or tight folding. Similar zones of intense deformation with large outcrop-scale offsets have been observed also elsewhere, allowing the definition of new major tectonic contacts that are relevant at map scale. Furthermore, in order to understand the regional effects and superposition, we have also measured deformation at farther distances from major faults of shear zones (black faults in Figs. 5, 7, 8 and 10).

Deformation has a brittle character in most observed situations. The pre-Mesozoic basement contains ductile shearing and greenschist facies metamorphism in the Supragetic unit and greenschist to amphibolite facies metamorphism in the Getic unit. However, the Mesozoic sedimentary cover is generally not affected by this ductile deformation, with the exception of a low- to sub- greenschist metamorphic facies observed in the vicinity of the main Supragetic thrust. Field observations included measurements of foliations, fold axes and their geometry, brittle faults and shear zones, observations of tilting and rotations. The sense of shear along brittle faults and shear zones was derived from kinematic indicators such as slickensides (including calcite slickenfibres, grooves and other brittle lineations), Riedel shears and brittle shear bands, by taking into account confidence criteria and quality ranks (e.g., Angelier, 1994; Doblas, 1998; Sperner and Zweigel, 2010). Shear bands, sheared quartz aggregates and, less frequent, consistent asymmetry of folds (e.g., Simpson and Schmid, 1983) were used for inferring shear senses in ductile and brittle-ductile transitional fabrics. In few situations, a larger number of conjugate shears were measured in the main shear zone, which was particularly useful to derive the kinematics of foliated fault gouges. The fault-slip data was separated in the field by observations of consistency, superposition, reactivation of deformation, or using timing criteria. We paid particular attention to syn- and post-kinematic sedimentation, used as a key timing indicator for the observed deformation stages, the most important being related to the fault-controlled deposition observed in Oligocene–Neogene sediments (Fig. 2). Further timing indicators observed in the field are structural cross-cutting, tilting and truncation relationships, which aided to understand the structural superposition.

The analysis of the obtained kinematic dataset has resulted in the definition of five deformation types (Figs. 5, 7, 8 and 10), grouped by the interpretation of three tectonic events, which respect all timing and superposition criteria observed in the field or otherwise available in studies of the neighbouring Serbo–Macedonian, Dinarides, Pannonian Basin and Morava Valley Corridor units (e.g., Erak et al., 2017; Matenco and Radivojević, 2012; Stojadinovic et al., 2013, 2017). We furthermore focussed on understanding the partitioning of strain in observed major faults or shear zones, by assigning the kinematics observed in multiple outcrops along the fault strike to its specific expression at map scale. The lateral correlation between outcrops is based on the character of deformation in similar lithologies (e.g., brittle fault gouges versus individual fault planes or brittle shear bands) as well as on the compatibility of deformation and offsets observed in the field with the one at map scale. The lateral correlation has demonstrated that the thrusting observed at the Supragetic and Upper Getic nappe contacts has an overall curved geometry in map view and is associated with the coeval formation of a large number of tear faults (Figs. 5 7, 10). We note that such tear-faults are perpendicular to and connect thrusting segments by accommodating their differential offsets in major shear zones. These tear faults are demonstrably different when compared with faults formed during the strike-slip deformation event (Fig. 8), which are widely observed outside major shear zones (see also Mladenović et al., 2019).

Our specific strain-based approach and the observed deformation are not entirely suitable to invert kinematic data to derive paleostress directions. Methodological limitations come from the fact that measurements in large offset shear zones do not satisfy the Wallace-Bott criteria and the often observed strain partitioning during deformation (such as thrusting associated with wedge and tear faulting, regional and local vertical axis rotations observed along drag folds) are well-known limitations of the paleostress methodology (e.g., Célérier et al., 2012; De Vicente et al., 2009; Hippolyte et al., 2012; Jones and Tanner, 1995; Orife and Lisle, 2003; Sperner and Zweigel, 2010). Reconstructing paleostress for such strain partitioning requires a high-resolution data set that is beyond the regional scope of our study. Nevertheless, in order to test the consistency of deformation at regional scale, we have also inverted our data by calculating paleostress tensors for all deformation that does not display strain partitioning effects and are located in the vicinity of large-offset faults. This means, for instance, that tear faulting and faults observed in outcrops to be associated with drag-folding rotations were not included in calculations. We have used the WinTensor software (Delvaux and Sperner, 2003) to calculate and optimise reduced paleostress tensors (Figs. A.1, A.2 and Table A.1 of the Supplementary Appendix) by following a standard inversion approach with confidence criterion (e.g., Angelier, 1994; Angelier and Goguel, 1979; Angelier and Mechler, 1977; Delvaux and Sperner, 2003 and references therein) and allowing a slip tolerance of ±26° (Lisle, 2013). Displacements along observed faults and calculated rotations are used as independent constraints to correlate with the paleostress tensors, which are interpreted to be part of the material response to imposed boundary conditions (e.g., Tikoff and Wojtal, 1999). Given the two approaches (strain and stress), we specifically use in interpretation a terminology that differentiates between stress calculations (compression-tension) and strain observations (contraction-extension).

Data were furthermore grouped and used in the construction of five regional cross sections (Fig. 4), where the surface kinematics was projected at depth and correlated with other existing surface and depth constraints. The eastern part of these profiles has less structural control at depth and, therefore, our surface to depth projection has a higher degree of uncertainty.

3.1. NW-SE to NE-SW oriented shortening in the vicinity of the Supragetic thrust

Although less extensive, the first set of structures are dominantly located along or in the vicinity of the Supragetic thrust and in all situations the observed faults and folds do not deform and are buried beneath the sediments of the overlying upper Oligocene - Miocene basins (Fig. 5). These structures are more frequent in the northernmost and the southern segments of the studied area (near Golubac and Kučevo in the north and east of Paraćin in the south, Fig. 5), being truncated at outcrop and map scale by all other subsequent deformation. The

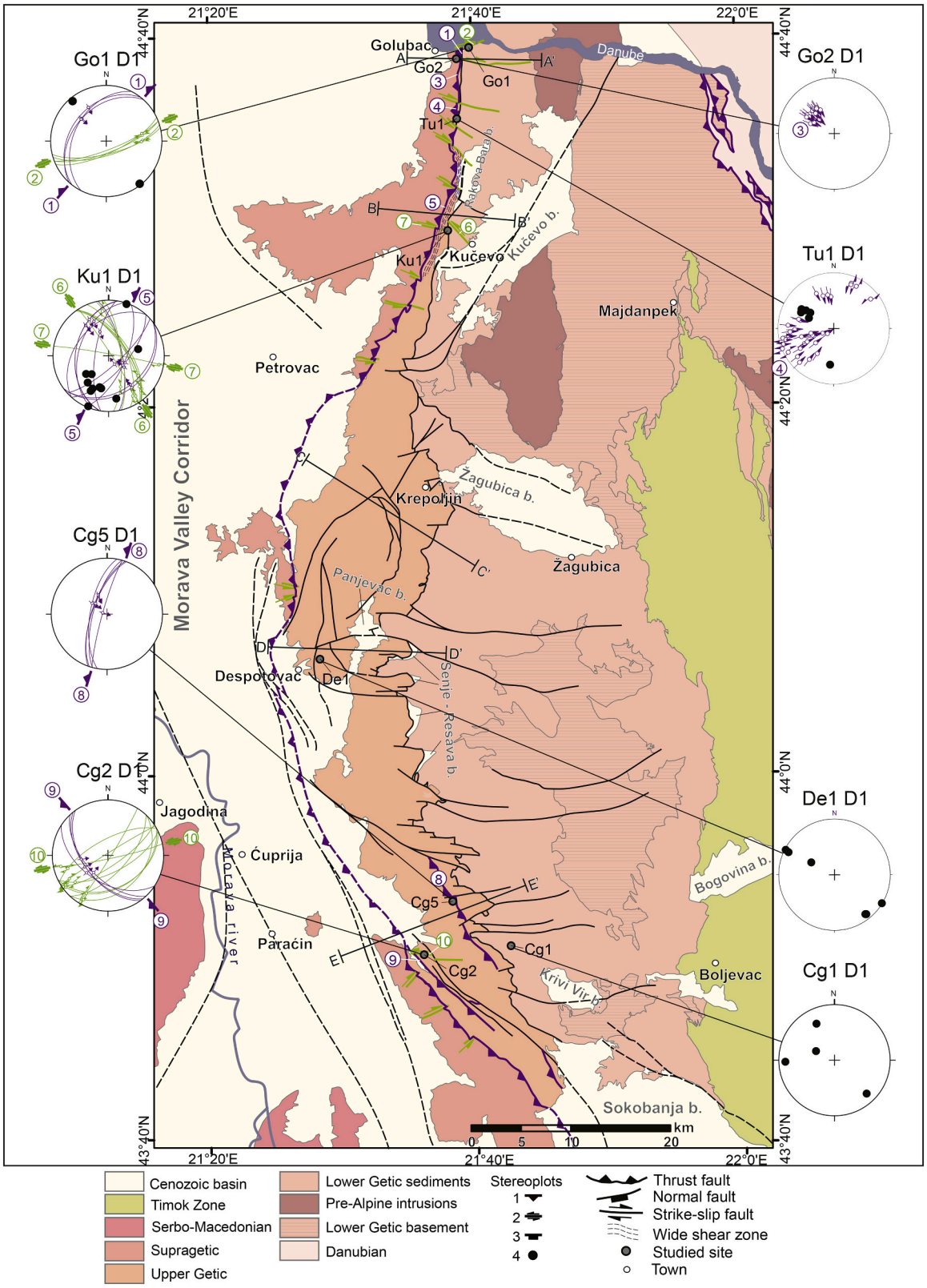

Fig. 5. Lower hemisphere stereoplots structures associated to Cretaceous shortening, plotted on the tectonic map of the studied area (complied after Kräutner and Krstić et al. (2003) and Basic geological map of former Yugoslavia, scale 1:100.000). Faults colored in purple are thrusts active during this phase, light green faults are active strike-slip faults, while black faults are other major faults in the area. Suggested faults or faults covered by Neogene sediments are dashed. Dark green straight lines indicate positions of cross sections in Fig. 4. Numbered structures in stereoplots are linked to map structures with the same number. Stereoplots legend: 1-thrust fault, 2-strike-slip fault, 3-normal fault, 4-fold axis. Note that plots Go2 D1 and Tu1 D1 show stretching lineations with sense of shear. (For interpretation of the references to colour in this figure legend, the reader is referred to the web version of this article.)

Paleozoic basement of the Supragetic unit and the neighbouring Mesozoic limestones of the Upper Getic sub-unit are affected by a deformation characterized by moderate- to high-angle thrusts. These thrusts are oriented NE-SW in the northern part of the studied area and have a top to SE - E oriented tectonic transport (structures 1, 3, 4, 5 in Fig. 5) which changes to NW-SE and top to NE in the southern part (e.g., structure 9 in Fig. 5), although some local variability is recognized at farther distances from the Supragetic thrust (structure 8 in Fig. 5). These two different orientations of thrusts are not observed in the same location. Thrusting is associated with numerous sub-vertical strike-slip faults (structures 2, 6, 7, 10 in Fig. 5), whose orientation in outcrops and at map scale is generally perpendicular to the ones of the map-scale thrusts.

In more detail, deformation at or near the Supragetic thrust is more intense and indicates a different degree of burial of its hanging-wall and footwall. An up to a few tens of meters thick low-grade metamorphic (low to very low greenschist facies) to cataclastic shear zone was observed in the Paleozoic metamorphics of the hanging-wall. This hanging-wall is affected by pervasive shearing, where a stretching lineation is observed to be associated with shear-bands and/or sigma clasts affecting oriented quartz aggregates (structures 3 and 4 in Fig. 5).

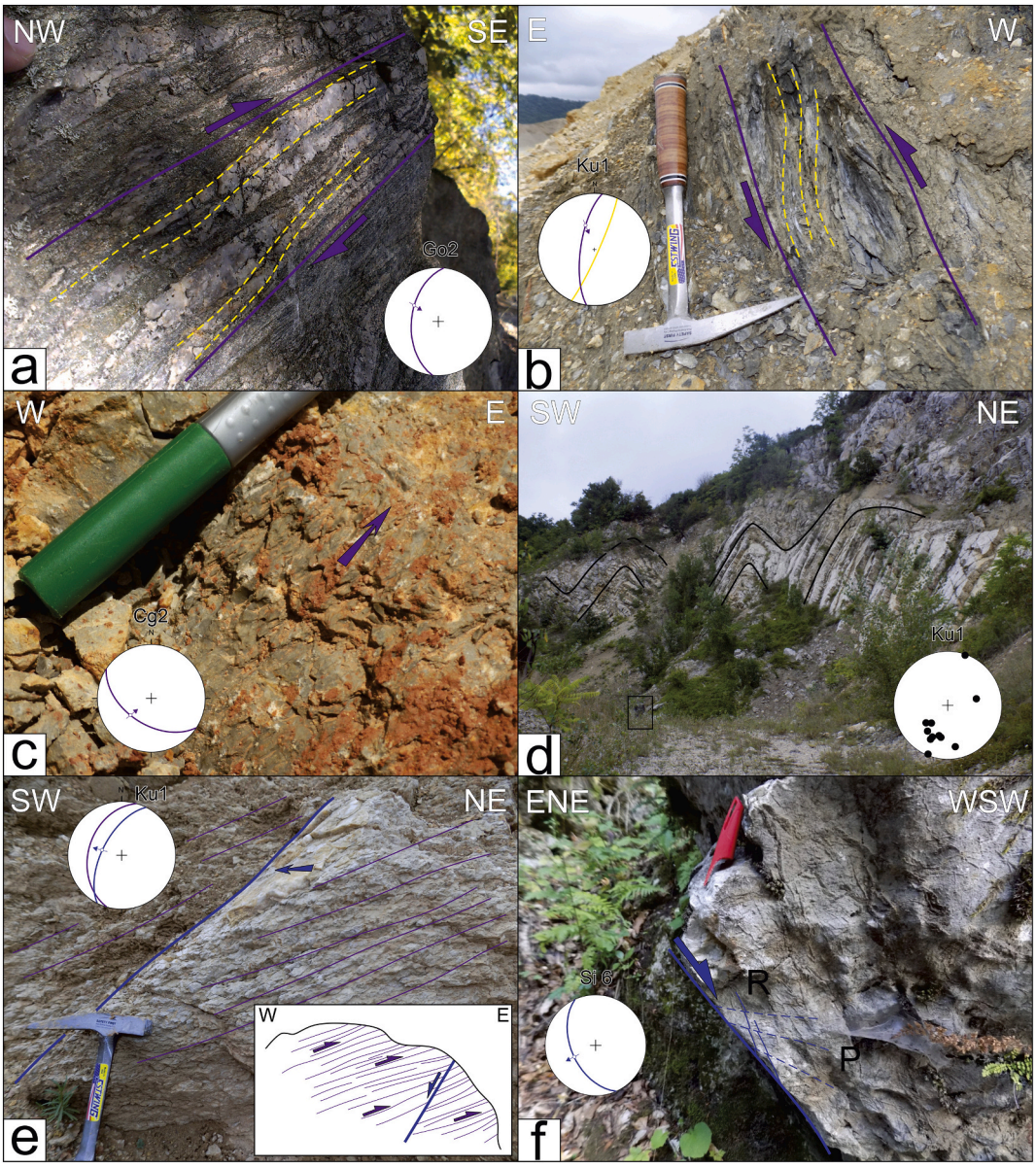

Fig. 6. Interpreted field photos of ductile to cataclastic structures associated with the late Early Cretaceous thrusting and subsequent Paleogene–Miocene orogen-perpendicular extension. Orientation of each photo is indicated in the upper right and upper left corners. Structures in the photos are plotted in stereoplots. Purple arrows and half arrows illustrate kinematics of interpreted structures related to the Cretaceous deformation, and blue ones indicate kinematics of subsequent extensional structures. a) Top to SE ductile thrusting in Supragetic unit metamorphic basement. Studied site Go2. b) Shear bands with reverse sense of shear in Upper Getic sub-unit Tithonian limestones. These form a cataclastic C—S fabric. Studied site Ku1. c) Fault plane with stylolites as kinematic indicators demonstrating top to NE thrusting. Studied site Cg2. d) Asymmetric decameter scale folds (see a standing man in black rectangle for scale) in Tithonian limestones of the Upper Getic sub-unit in the footwall of the Supragetic thrust. Black lines represent bedding. Fold axes are plotted in lower hemisphere stereoplot. Vergence of the folds indicates top to SE thrusting. Studied site Ku1. e) Normal fault (blue arrow illustrates the relative hanging wall movement) truncating the cataclastic shear zone (purple lines) formed in Tithonian limestones in the footwall of the Supragetic thrust. Studied site Ku1. Inset: Outcrop-scale cross-section sketch of relationship between thrusting related foliation (purple lines and half arrows) and N-S oriented normal fault (blue half arrow). f) Normal fault with associated R and P Riedel shears, indicating NE-SW oriented orogen-perpendicular extension in Tithonian limestones at the studied site Si6. (For interpretation of the references to colour in this figure legend, the reader is referred to the web version of this article.)

For example, in the northern area near Golubac, such hanging-wall shearing in quartz aggregates is associated with a top to SE direction of tectonic transport (e.g., structure 3 in Fig. 5 and Fig. 6a). This shearing is sub-parallel with the dominantly W-dipping foliation of the Supragetic metamorphics. Often decimeters thick shear zones are observed affecting the Mesozoic limestones located in the immediate footwall of the Supragetic thrust (structure 5 in Fig. 5 and Fig. 6b). In the northern part of the studied area, deformation along these shear zones indicates thrusting with a dominant top-SE to E direction of tectonic transport, locally associated with NW-vergent backthrusts (structure 5 in Fig. 5), or with *E*-W to NW-SE oriented strike-slip faulting observed by conjugate Riedels in the main shear zone (site Ku1, structures 6 and 7 in Fig. 5). In the southern part of the studied area, the overall deformation changes to NW-SE oriented thrusts or shear-zones that have a dominant NE direction of tectonic transport (structure 9 in Fig. 5 and Fig. 6c) and are associated with N*E*-SW oriented strike-slip faults, cross-cut at map scale by subsequent strike-slip deformation (structure 10 in Fig. 5). The sense of shear along closely spaced thrusts truncating Tithonian limestones in the footwall of the Supragetic thrust is often derived from *syn*-kinematic growth of calcite fibers, grooves and centimeter-scale stylolites (an example is shown in Fig. 6c).

The character of deformation changes at farther distances (few hundred meters) in the footwall of the Supragetic thrust, where the pervasive shearing is replaced by meter-scale, slightly asymmetric folds that are oriented N*E*-SW and have a SE vergence in the northern part of the studied area (e.g., site Ku1 in Fig. 5 and Fig. 6d). The same asymmetric folds are oriented NW-SE with NE vergence in the southern part of the studied area, although the number of measurements is rather limited (e.g., site Cg1, Fig. 5). At farther (kilometres) distances, few high-angle reverse faults are observed in this footwall, which are truncated by subsequent normal faults in outcrops and map scale (structure 8 in Fig. 5 and structure 14 in Fig. 7).

3.2. *Multi-geometry extension and strike-slip*

Superposition criteria and truncation of the upper Oligocene – Miocene basins indicate that the Supragetic thrusting is followed in time by three types of structures. The first type of structures are N-S oriented, dominantly W-dipping normal faults, which are observed more frequently in the field near the contact with the Morava Valley Corridor and in the vicinity of the Upper Getic thrust contact (dark blue in Fig. 7). These faults often truncate the previously described thrusts, as observed near Kučevo (site Ku1, structure 2 in Fig. 7). Here, the previously formed cataclastic foliation in the footwall of the Supragetic thrust is cross-cut in one example by a W-dipping normal fault (Fig. 6e). Outside main shear or fault zones, this deformation is observed along individual fault planes or Riedel shears by calcite slickenfibres, such as the top to SW normal faulting in Tithonian limestones of the Upper Getic sub-unit at site Si6 (Figs. 6f and 7). The strike of outcrop-scale normal faults and associated map-scale shear zones gradually changes southwards from N-S in the northern part of the studied area to NNW-SSE and NW-SE, with some local variations. This change follows the regional change in strike of the main nappe contacts, while generally remaining (sub-)parallel to them, normal faults being observed both above and below the thrusts at outcrop scale. Map-scale normal faulting can be documented only in the vicinity of the Morava Valley Corridor and Upper Getic thrust contact, more frequent in the areas of Krepoljin and Despotovac (structures 4–7 and 9–10 in Fig. 7). The sense of shear is dominant top-W and top-E north of Despotovac and top- WSW to SW southwards, although the number of available observations in the latter area is reduced. A higher density of such normal faults is observed near the Senje–Resava Basin, where they appear to control the Oligocene–early Miocene sedimentation (e.g., sites De9 and Cg7, structures 10 and 13 in Fig. 7) and are truncated by the subsequent Upper Getic thrusting, as explained below. The number and offset of such normal faults indicating orogen-perpendicular extension decrease eastwards, at farther distances from the Morava Valley Corridor and the Upper Getic thrust contact.

The second type of structures observed is made up of a large number of strike-slip faults (Fig. 8), which are distributed in the entire studied area and have variable kinematics from pure strike-slip to oblique-slip. This strike-slip deformation is dominantly dextral, with NN*E*-SSW to N-S oriented faults in the northern and central parts (Figs. 8, 9a,b) and further to NNW-SSE to NW-SE more southwards in the studied area (Figs. 8, 9c). Conjugate sinistral faults are commonly observed, varying in orientation from N*E*-SW to N-S oriented faults (Figs. 8, 9d). This change in orientation of outcrop-scale strike-slip faults also follows the general change in strike of the main nappes contact from north to south, although local variations are also observed (Fig. 8). The character of this deformation is variable, from breccias and fault gouges in up to 50 cm wide shear zones to localized shears along individual fault planes (e.g., Fig. 9a–d). These strike-slip faults were found locally to truncate or reactivate the older mylonitic to cataclastic foliation that formed at the Supragetic unit thrust contact. For example, in location Tu1 (structure 1 in Fig. 8) the reactivation is visible by dm-scale dextral shearing and mineral growth along individual fault planes (Fig. 9a) truncating the ductile to cataclastic foliation of the W-ward dipping high-angle shear fabric of Tithonian limestones. However, most often such strike slip deformation is observed along isolated faults that cannot be connected with regional structures and stratigraphic offsets, such as for instance in vicinity of the Upper Getic thrust at site De9, where a decimetre to meter scale sub-vertical dextral fault deforms Lower Cretaceous limestones (Figs. 8 and 9b). Strike-slip kinematics is well visible in fault gouges, such as NW-SE oriented dextral strike-slip fault in Cg2 (Figs. 8 and 9c), or along thick slickensides or calcite slickenfibres, such as a NNE-SSW oriented sinistral fault observed in Tithonian limestones at site Gk3 (Figs. 8 and 9d). Despite the fact that outcrop kinematics is characterized often by a large number of isolated faults measured in the field, these are associated with only with a few regional, map-scale dextral shear zones (Fig. 8). These shear zones are N-S to NNE-SSW oriented near Golubac and Kučevo in the north (structures 1 and 2 in Fig. 8) and NW-SE in the south, as observed SE of Paraćin (structure 3 in Fig. 8).

The third type of structures observed in the field consists of *E*-W oriented normal faults that are perpendicular to the orogenic strike and indicate orogen-parallel extension (light blue in Fig. 7). Conjugated N- and S- dipping normal faults were observed in outcrops and can be associated with regional, map-scale shear zones. In outcrops, this deformation is characterized by individual fault planes, or by fault breccias or meters thick foliated fault gauges, when the observed offset is larger. These faults are associated with syn-kinematic sedimentation, such as observed in the middle–upper Miocene sediments of the Panjevac Basin (site De4, structure 8 in Fig. 7; see also Antonijević et al., 1970), where coarser wedge-shaped sediments were deposited only in the hanging-wall of *E*-W oriented normal faults that were overlain by deeper water sedimentation (Fig. 9e). These normal faults truncate earlier formed reverse faults, as observed in the Permian sandstones of the Upper Getic thrust (e.g., site Cg5, structure 14 in Fig. 7), where such truncation is observed along low-angle normal faults that indicate N-S extension (Fig. 9f). In other locations, these normal faults reactivate E-W oriented strike-slip faults belonging to the first deformation event (e.g., structures 1 and 3 in Fig. 7), such as observed in Upper Jurassic limestones of the Lower Getic sub-unit (site Go1, structure 1 Figs. 7 and 9g). In this site, E-W oriented normal faults create a fault gauge breccia that contains planes with inherited sub-horizontal dextral strike-slip slickensides. Interestingly, the E-W oriented normal faults and N-S oriented strike-slip faults overprint each other in outcrop kinematics, observed often in the vicinity of such normal fault with large, map scale offset (e.g., site De3, Figs. 7, 8 and 9h). Such an interplay between normal faulting and strike-slip infers that the two types of deformation formed during the same tectonic event. In map view, regional E-W oriented normal faults border many of the Neogene basins, where they control the early middle Miocene sedimentation and are overlain by younger deposits (Figs. 2 and 7). These faults are also associated with tilting and

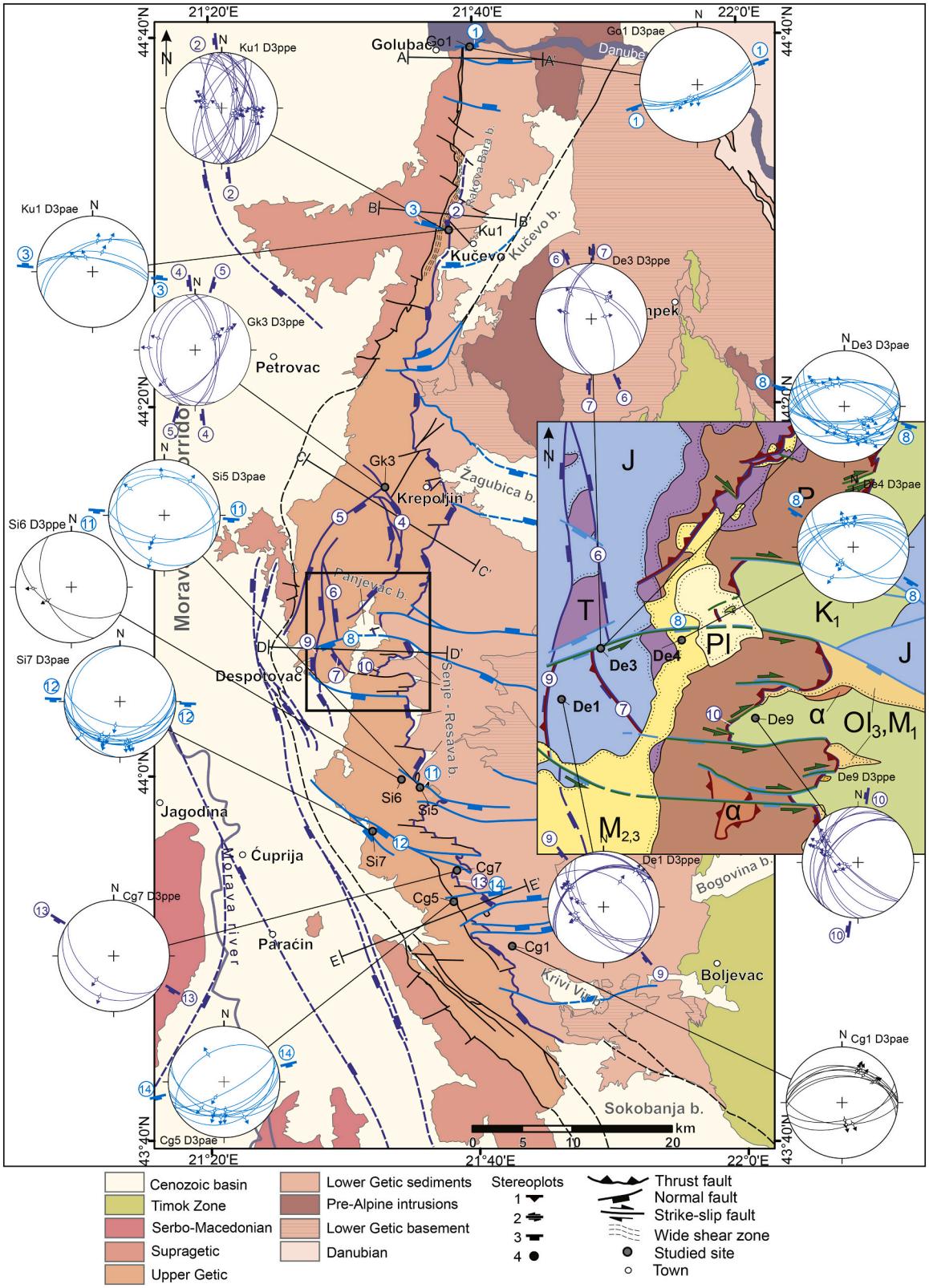

Fig. 7. Map of the studied area (same conventions as in Fig. 5) with lower hemisphere stereoplots of structures associated to Oligocene–Miocene orogen-perpendicular and orogen-parallel extension. Faults colored in dark and light blue are activated by these extensions, respectively. Black faults are other major faults in the area. Suggested faults or faults covered by Neogene sediments are dashed. Black rectangle shows the position of the inset in right part of the figure. Inset: Simplified geological map of a segment of the Senje-Resava Basin thrusted by Permian sediments of Upper Getic sub-unit (simplified and modified after Basic geological map of former Yugoslavia, scale 1:100.000 and data from this study). P-Permian red clastics; T-Triassic clastics and limestones; J-Jurassic clastics and limestones; K_1-Lower Cretaceous limestones and marls; α-Upper Cretaceous Banatites; Ol_3,M_1-upper Oligocene to lower Miocene sediments of Senje-Resava Basin; $M_{2,3}$-middle to upper Miocene sediments of Morava Valley Corridor and adjacent basins; Pl-Pliocene conglomerates and travertine. (For interpretation of the references to colour in this figure legend, the reader is referred to the web version of this article.)

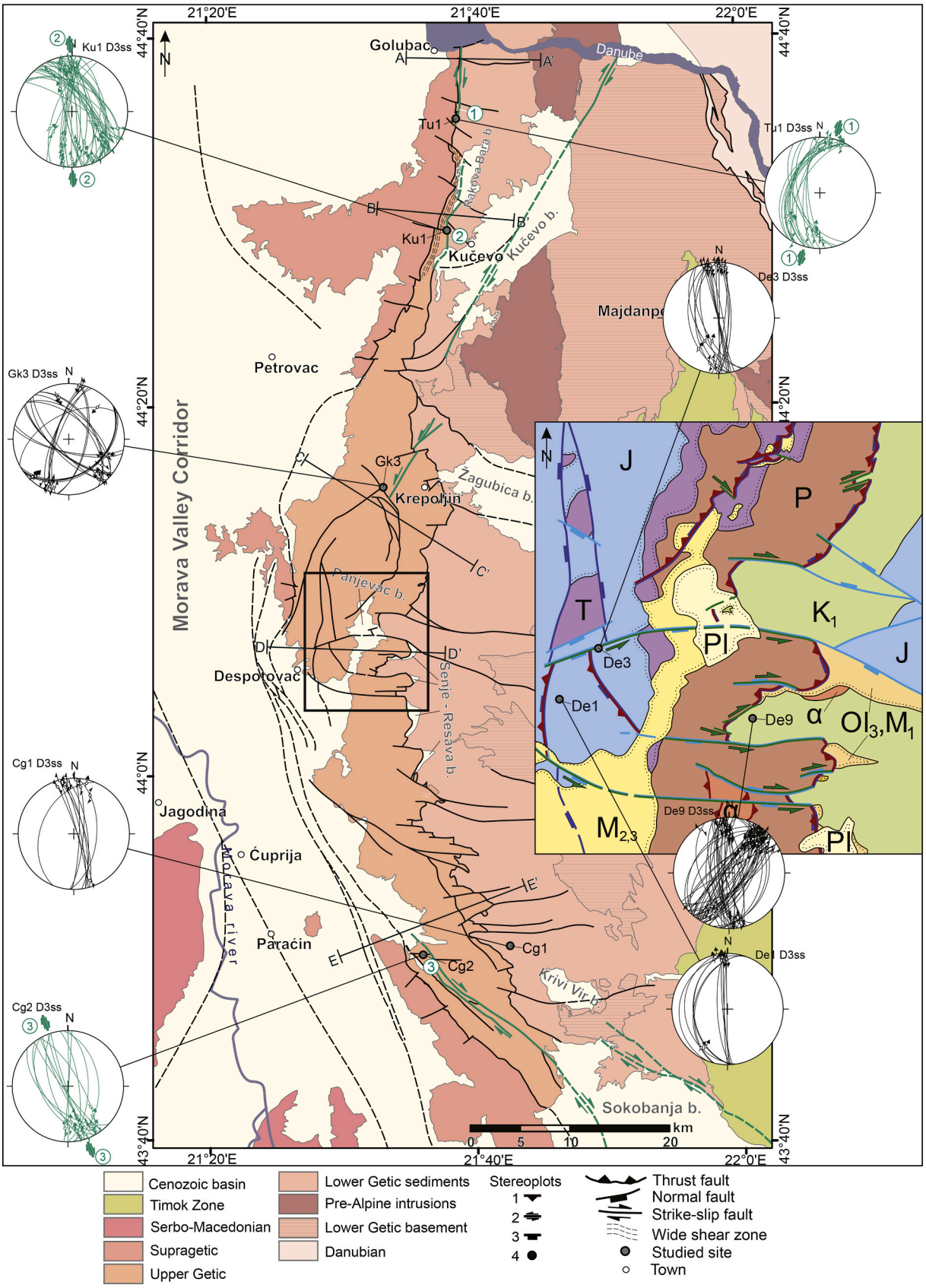

Fig. 8. Map of the studied area (same conventions as in Fig. 5, inset is same as in Fig. 7) with lower hemisphere stereoplots of structures associated to regional strike-slip deformation. Faults colored in green are active during this phase. Black faults are other major faults in the area. Suggested faults or faults covered by Neogene sediments are dashed. (For interpretation of the references to colour in this figure legend, the reader is referred to the web version of this article.)

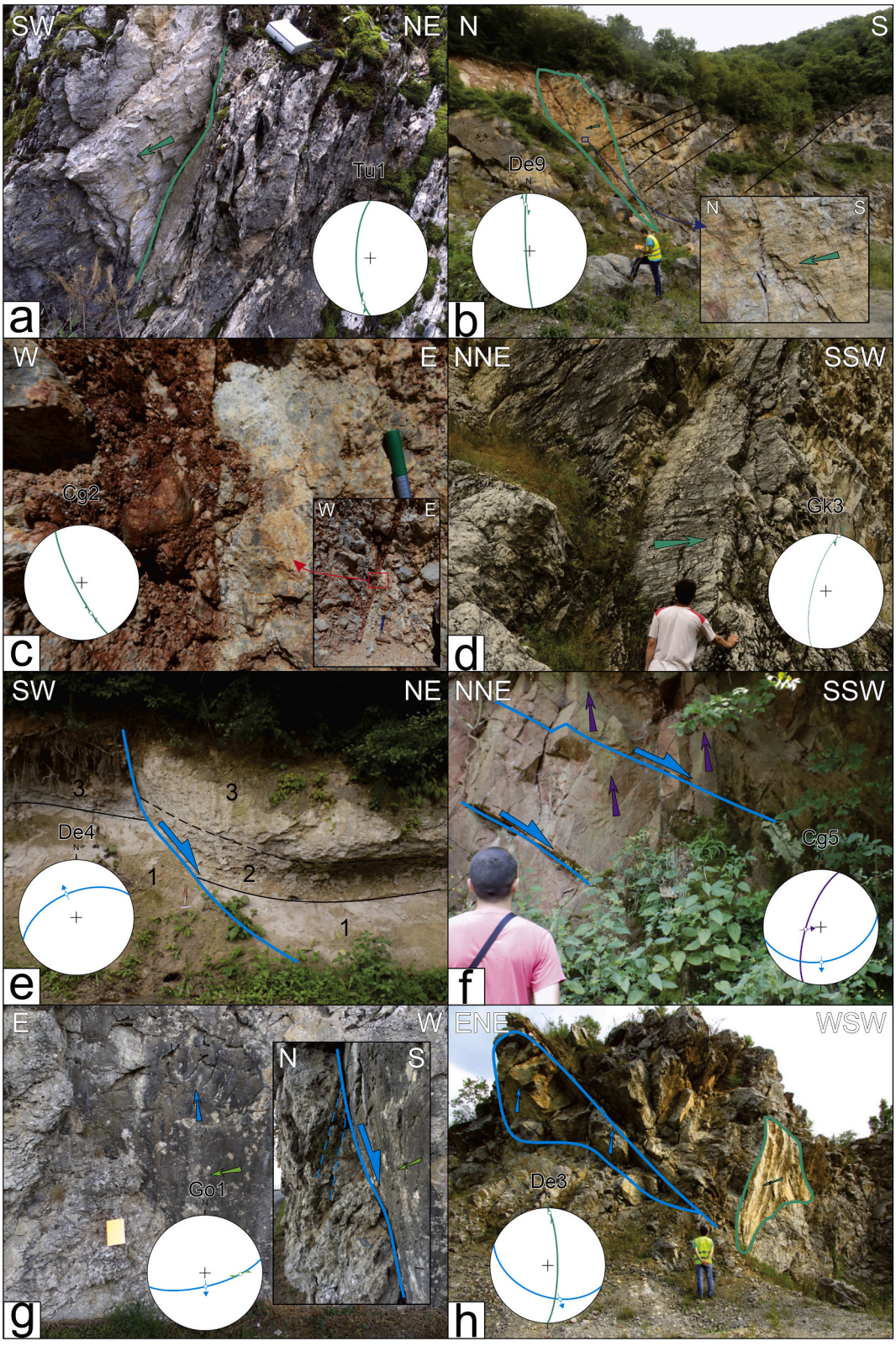

(caption on next page)

Fig. 9. Interpreted field photos of brittle structures related to Paleogene to Miocene deformation. Orientation of each photo is indicated in the upper right and upper left corners. Structures in the photos are plotted in stereoplots. a) Dextral, N-S oriented strike-slip fault (green arrow) truncating older thrusting related foliation in weakly metamorphosed Upper Jurassic limestones of the Upper Getic sub-unit. Studied site Tu1. b) Dextral, N-S oriented strike-slip fault offsetting tilted Lower Cretaceous limestones (black lines indicate bedding position) of the Lower Getic sub-unit at studied site De9. Inset illustrates the fault surface in detail with striations that indicate dextral shearing (green arrow shows the relative movement of the missing block). c) Fault breccia associated to NW-SE oriented dextral strike-slip fault zone at location Cg2. d) NNE-SSW oriented sinistral fault in Tithonian limestones. Studied site Gk3. e) Syn-kinematic sedimentation in the hanging wall of a normal fault during orogen-parallel extension (blue half arrow) in the middle to upper Miocene sediments (1-sandy siltstones, 2-conglomerates, 3-marls, dashed line indicates gradual transition from conglomerates to marls). Studied site De4. f) Outcrop of Permian sandstones of the Upper Getic sub-unit demonstrating normal faults activated by orogen-parallel extension (blue half arrows) truncating high angle reverse faults interpreted as a result of late Early Cretaceous thrusting (dipping towards camera, purple arrows). Studied site Cg5. g) Dextral, ENE-WSW oriented strike-slip fault with weakly preserved striations (light green arrow indicates relative movement of the footwall) that was reactivated by orogen-parallel extension as documented by Riedel shears in fault breccia (inset, blue half arrow). Studied site Go1. h) N-S oriented dextral fault (green arrow illustrates relative movement of the missing block) and ESE-WNW oriented normal fault (blue arrow indicates relative movement of the footwall). Interaction and superposition of faults are not clear. Studied site De3. (For interpretation of the references to colour in this figure legend, the reader is referred to the web version of this article.)

exhumation of the metamorphosed Paleozoic sediments in their footwall (Fig. 7), suggesting a listric or block tilting geometry. These bordering normal faults decrease their offsets laterally along their strike, which imply increased amounts of extension in the centre of the Lower Getic sub-unit, in the place where the Paleozoic metamorphosed basement is more widely exposed (Fig. 7).

We note that these three sets of normal and strike-slip faults could have been formed during three successive deformation events, partly overlapping, or they can belong to the same event by distributing the strain along differently oriented structures. Available superposition timing criteria are not fully diagnostic.

3.3. Top-E thrusting of the Upper Getic sub-unit

Superposition criteria indicate that the youngest deformation type is associated with a large number of reverse faults with E-ward vergence that are associated in map view with the thrusting of the Upper Getic sub-unit (commonly Permian red sandstones) over the Lower Getic sub-unit, commonly made up in outcrops by Lower Cretaceous limestones and the upper Oligocene–lower Miocene sediments of the Senje–Resava Basin (Figs. 2 and 10). Two sets of structures were observed in the field in map-scale shear zones.

The first set of structures is thrusts or oblique-reverse faults that are dominantly top-E and are observed along the Upper Getic thrust and its vicinity (e.g., structures 1, 2, 4, 6, 7, 10 and 13 in Fig. 10). This Upper Getic thrust is generally high angle where Permian sandstones are thrust over Lower Cretaceous limestones (e.g., site Si5, Figs. 10 and 11a). Although the thrust itself is rarely exposed, its kinematics is obvious in the immediately adjacent rocks affected by the wider shear zone (e.g. site De6, Figs. 10, 11b, c). The same structure is low angle when it is thrusted over the poorly consolidated upper Oligocene to lower Miocene sediments of the Senje–Resava Basin. These sediments do not create foliated fault gouges or other types of shear zones where kinematics can be measured. However, the kinematics of the contact can be measured in the in Permian - Mesozoic rocks affected by the shear zone in the hanging-wall or at farther distances in the footwall, while its geometry can be derived from the topographic expression (e.g., Fig. 11d). Interesting is that *E*-vergent thrusting over the upper Oligocene – Miocene sediments reactivate often earlier orogen-perpendicular normal faults (e.g., structure 2 in Fig. 10).

The second set of structures is observed in outcrops along numerous strike-slip faults (Fig. 10), where they are always associated with roughly E-W oriented map-scale shear-zones that connect various segments of the Upper Getic thrust and are both dextral and sinistral (structures 3, 5, 8, 9, 11, 12, 14–19 in Fig. 10). The orientation and sense of shear of the strike-slip faults measured in outcrops mirrors the ones of the *E*-W oriented map-scale faults, while often conjugates are observed (such as in the case of structures 12, 15 and 19 in Fig. 10). These strike-slip faults are generally perpendicular to the orientation of the Upper Getic thrust when offsetting this structure, while locally changing their strike towards NW-SE or N*E*-SW at farther distances. Typically, such strike-slip faults offset the Upper Getic thrust with 1–5 km (e.g., structure 14 in Fig. 10 and site De10, Fig. 11e), while outcrop kinematics is often derived from large Riedel shears (Figs. 11e, f).

Interestingly, measurements of bedding and the geometry of faults show vertical axis rotation in the vicinity of strike-slip faults due to local drag-folding, where differently oriented faults with the same kinematics are situated in the immediate vicinity. This situation is visible, for example, in site De9 (Fig. 10), where *E*-W oriented dextral strike-slip faults are rotated clockwise by dragging along a higher offset, NE-SW oriented dextral fault (structure 12, black and green respectively in plot De9 D4, Fig. 10).

4. Interpretation

The results of the kinematic study show a complex poly-phase tectonic evolution of the studied segment of Serbian Carpathians that reflects the formation of the highly bended Dacia Mega-Unit of the Carpatho–Balkanides overprinted by Dinarides orogenic processes. Although many structural elements are common with neighbouring segments of the South Carpathians and Balkanides, a number of deformation stages are specific to the studied area that relate in particular to multi-phase extension, strike-slip deformation and vertical axis rotations.

4.1. Cretaceous nappe emplacement

The oldest phase of contraction led to the nappe emplacement of the Supragetic unit that was associated with tear faulting (Fig. 5). Structures observed in this unit indicate that the onset of thrusting was associated with transitional ductile-brittle deformation that is cross-cut in later stages by brittle thrusts or tear faults. Such a succession of deformation during the same tectonic event indicates exhumation of the Supragetic unit during thrusting. This interpretation is in agreement with the observation of ductile structures at the Supragetic/Getic contact in the South Carpathians, dated at 120 Ma (Dallmeyer et al., 1996). Alternatively, one can interpret the ductile structures to be formed during an older Variscan event, while only the brittle ones formed during the Cretaceous thrusting. However, the ductile to brittle structures have the same kinematics, while the continuous exhumation is justified by the offset and geometry of Paleozoic-Mesozoic strata truncated by the Supragetic thrust (Fig. 4). Although the Cretaceous offset along the Supragetic thrust is difficult to estimate due to the absence of reliable markers, the transition from ductile to brittle deformation during thrusting indicates a minimum of 10–15 km offset. The youngest sediments affected by this thrusting are Lower Cretaceous limestones (Fig. 3), while the Supragetic thrust contact is truncated by all subsequent deformation and is often covered by Oligocene - Miocene sediments of the Morava Valley Corridor (Fig. 5).

Outcrops and regional cross-sections indicate that thrusting was associated with the formation of E-vergent folds and a wide shear zone at the Supragetic thrust contact that recorded splaying by the formation of

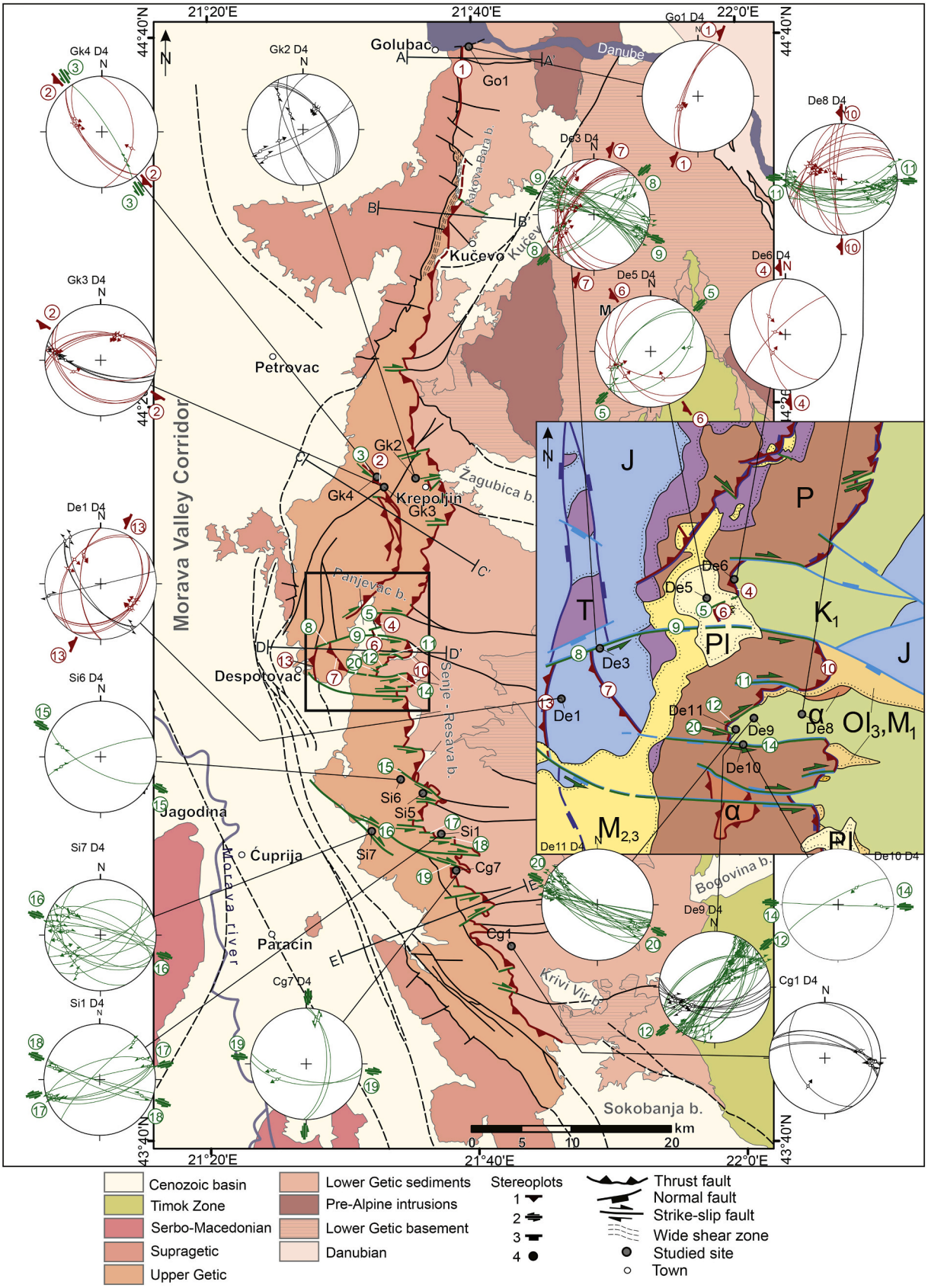

Fig. 10. Map of the studied area (same conventions as in Fig. 5, inset is same as in Fig. 7) with lower hemisphere stereoplots of structures associated to late Miocene shortening. Faults colored in red are active thrusts during this contraction and green faults are active strike-slip faults. Black faults are other major faults in the area. Suggested faults or faults covered by Neogene sediments are dashed. (For interpretation of the references to colour in this figure legend, the reader is referred to the web version of this article.)

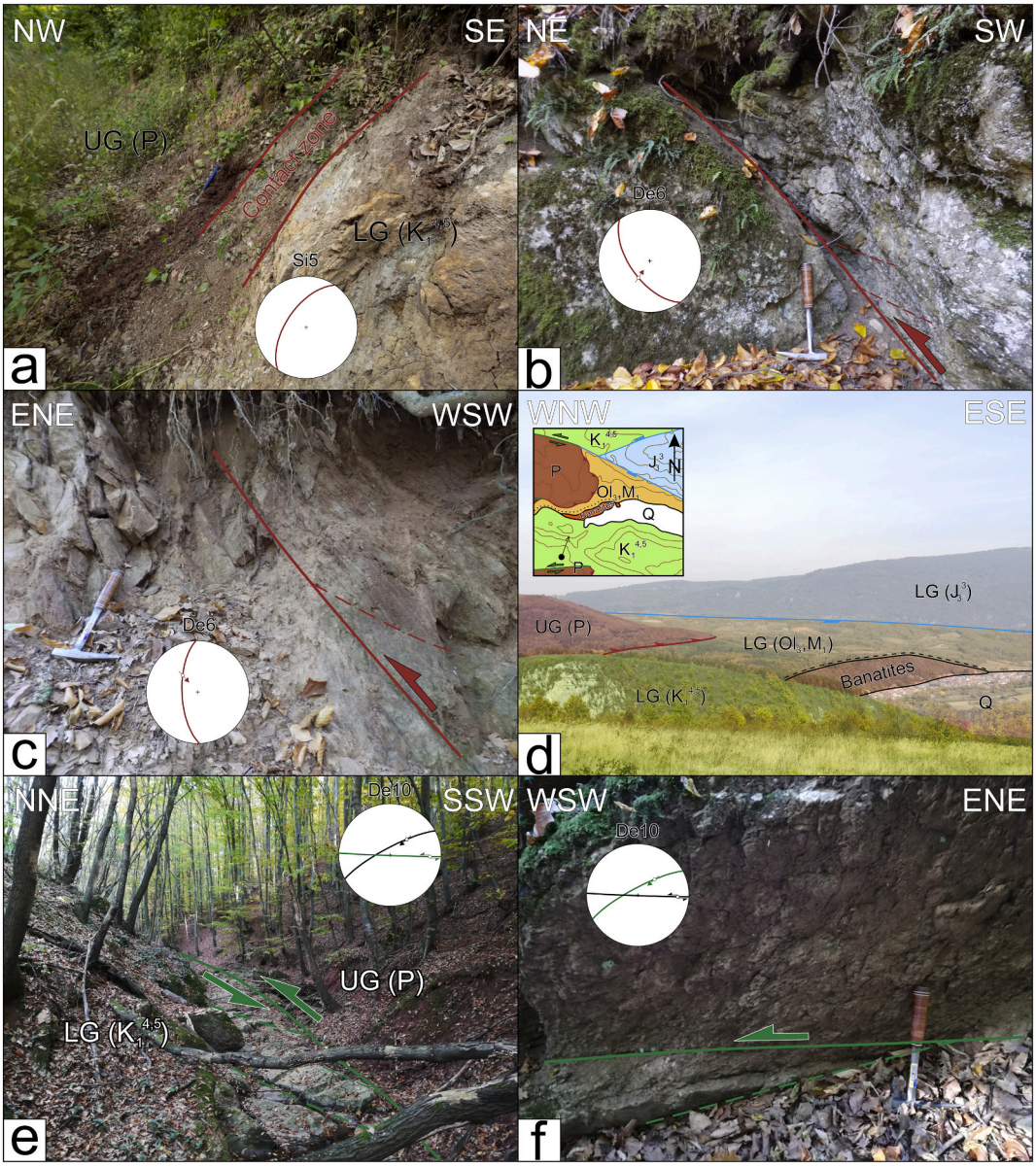

Fig. 11. Interpreted field photos of structures related to the Upper Getic thrust. Orientation of each photo is indicated in the upper right and upper left corners. Structures in the photos are plotted in stereoplots. UG-Upper Getic sub-unit; LG-Lower Getic sub-unit; P-Permian sandstones; J_3^3-Tithonian limestones; $K_1^{4,5}$-Barremian–Aptian limestones; Banatites - Upper Cretaceous subvolcanic intrusion; Ol_3,M_1-upper Oligocene to lower Miocene sediments; Q-Quaternary sediments; a) Upper and Lower Getic sub-units in a high angle contact at studied site Si5. b) Lower Cretaceous limestones of the Lower Getic sub-unit in the footwall of the Upper Getic thrust, few meters away from UG/LG contact. Studied site De6. c) Permian sandstones of the Upper Getic sub-unit, few meters away from UG/LG contact in the hanging wall of the thrust. Studied site De6. d) Interpreted landscape view of the Upper Getic thrust. Note the low angle geometry of the thrust with footwall represented by early Miocene sedimentary sequence of the coal-bearing Senje–Resava Basin. Inset illustrates simplified geological map of the area shown in the photo (modified after Basic geological map of former Yugoslavia, scale 1:100.000) with the position of the camera (black dot) and the azimuth of camera view (black arrow). e) Subvertical sinistral strike-slip fault (thick green line, green great circle in stereoplot) accommodating different offsets of the Upper Getic thrust segments north and south of the fault. Riedel shears are associated with this fault (dashed green lines, black great circle in stereoplot)and are defining sense of shear along this major fault. Studied site De10. f) Sinistral strike-slip fault (green great circle in stereoplot) as one of the Riedel shears form Fig. 11e. Studied site De10. (For interpretation of the references to colour in this figure legend, the reader is referred to the web version of this article.)

trailing imbricated fans in the Upper Getic footwall (Fig. 4). The Supragetic thrusting has a flat-ramp geometry (e.g., Fig. 4a) that changes its offset along the orogenic strike (compare cross-sections in Figs. 4a, b, e). Changes in offset are accommodated by the formation of ~*E*-W oriented sub-vertical tear faults and lateral ramps (Fig. 5). A similar deformation style by the formation of ramp-folds, fault-propagation folds and asymmetric *E*-vergent folds is observed in the Upper Getic sub-unit. However, while the Supragetic thrust is covered by all Oligocene - Miocene sediments, the Upper Getic sub-unit thrusts with a large offset over these sediments (Figs. 4c–e) and has only a brittle character. This demonstrates that the thrusting of the two units took place during different deformation events, i.e. the Supragetic thrusting took place during the Cretaceous, while the Upper Getic thrusting took place during the late Miocene. However, it is also possible that the Upper Getic thrusting has been initiated during the Cretaceous by the low amount of offset observed in the north (Figs. 4a, b) by splaying in the footwall of the Supragetic thrust, while being reactivated during the late Miocene.

The overall transport direction of the Supragetic thrusting changes along the strike of the orogen from top-SE in the north to top-NE in the

south, remaining always perpendicular to the present oroclinal geometry of the nappes. This wide variation in thrusting direction does not reflect two separate shortening events, but the observed change in contraction direction is the result of vertical-axis rotations post-dating the main Cretaceous thrusting event. This rotation agrees with a gradual increase in subsequent Paleogene–Miocene clockwise vertical axis rotation from negligible in the Balkanides to 90° in the South Carpathians (Csontos and Vörös, 2004; van Hinsbergen et al., 2008). These differences in contraction direction observed in the studied area suggest that ~40° of differential Paleogene–Miocene clockwise rotations have been taken up by the Serbian Carpathians after the Cretaceous thrusting (Fig. 5).

4.2. Paleogene to middle Miocene interplay between bi-directional extension and strike-slip

Although not directly apparent in the large-scale structure of the studied Serbian Carpathians, our detailed field observations infer that three of the observed deformation types are in fact different structural responses formed during a long-lived tectonic event that post-dated the Cretaceous nappe stacking.

The first type are normal faults that are oriented (sub-)parallel to nappe contacts and are clustered in the western part of the studied area near the Supragetic and Upper Getic thrusts (dark blue in Fig. 7). These normal faults have a dominant W-ward dipping direction and are associated with the initial Oligocene - early Miocene extension observed in the Morava Valley Corridor, together with Senje–Resava, Panjevac and Bogovina basins (e.g., Figs. 2 and 4c–e, Erak et al., 2017; Mai, 1995; Matenco and Radivojević, 2012; Obradović and Vasić, 2007; Pavlović, 1997; Žujović, 1886). The large number of N-S oriented and W-dipping normal faults clustered in the immediate vicinity of the Upper Getic/Lower Getic contact indicates a larger amount of extension in the Morava Valley Corridor and the Senje–Resava Basin. It is likely that these two basins were initially continuous and part of a larger Morava Valley Corridor Oligocene - middle Miocene depositional area, being separated subsequently by the late Miocene thrusting of the Upper Getic sub-unit (Fig. 4c–e).

Based on all of these observations and correlations, we interpret that orogen-perpendicular extension has created the initial subsidence in the Morava Valley Corridor and the adjacent intramontane basins in the western part of the presently exposed Serbian Carpathians during Oligocene–early Miocene times. The change from E-W extension in the northern and central parts of the studied area to more NE-SW extension in the south follows the change in the orientation of main Supragetic and Getic units. Therefore, this change also indicates up to ~40° vertical-axis rotations largely post-dating the main extensional deformation.

The second type, strike-slip deformation has created NE-SW to NW-SE oriented dextral and sinistral faults that are distributed throughout the entire studied area at outcrop scale. The fact that only few map-scale faults with low offset can be attributed to this deformation (Fig. 8) indicate a diffused and/or distributed character of deformation, which is in agreement with previous observations (Mladenović et al., 2019). Outside the studied area, the kinematics and geometry of these outcrop-scale faults are compatible with the activation of the well-known and similarly 40°–80° curved large dextral strike-slip faults, the ~35 km offset late Oligocene Cerna Fault and ~ 65 km offset early Miocene – early middle Miocene Timok Fault (Fig. 2, Berza and Drăgănescu, 1988; Kräutner and Krstić, 2003). When compared with these large offset dextral faults, our kinematic observations indicate a similar change from NW-SE dextral in the south to more N-S dextral in the north associated with a compatible change in the direction of conjugate sinistral faults, although there is a significant variability between these directions across the entire studied area (Fig. 8). The differences in strike-slip directions between the north and the south show ~40° of clockwise rotations, while the variability of deformation indicate that strike-slip deformation took place before or during rotation.

The third type, orogen-parallel extensional structures, is associated with numerous outcrop-scale *E*-W oriented normal faults that can be directly correlated with larger offset (<1 km) regional E-W oriented normal faults and shear zones (light blue in Fig. 7). These normal faults truncate the Paleozoic basement in the centre of the studied area, while northwards and southwards they control the onset of early middle Miocene deposition in the Žagubica and Krivi Vir Basin. Furthermore, similar E-W oriented normal faults control the early middle Miocene onset of deposition in large intramontane basins outside our studied area, such as Sokobanja and Svrljig Basins and also, possibly, in the Bela Palanka Basin (Fig. 2). These basins have asymmetric, half-graben geometry that shows increasing subsidence towards the main controlling fault located southwards (Marović et al., 2007). With the notable exception of the Žagubica Basin that shows an WNW-ESE orientation (i.e. 20–30° clockwise rotation), all other basins and genetically associated faults are E-W oriented along the entire curved geometry of the Serbian Carpathians (Fig. 2). This observation suggests that the N-S oriented orogen parallel extension took place dominantly after the ~40° clockwise rotation.

Although our study cannot fully discriminate a complete superposition of events, all these observations indicate that the three deformation types (orogen- perpendicular and parallel normal faulting combined with strike-slip) developed successively, but partly overlapped in time. The late Oligocene onset of orogen-perpendicular extension largely predates the ~40° of clockwise rotation, the latest Oligocene-early middle Miocene stage of strike-slip took place during the clockwise rotation and the early Miocene–early middle Miocene stage of orogen-parallel extension largely postdates the clockwise rotation. All these three deformation types can be actually grouped in a continuous late Oligocene–early middle Miocene tectonic event that took place during the overall clockwise rotation of the Serbian Carpathians, accommodated by the 100 km cumulated offset of the curved Cerna-Timok Fault system. One can obtain the previously reported variable strike-slip paleostress stress field for the Oligocene - middle Miocene rotation of the Serbian Carpathians (Mladenović et al., 2019) by cumulating all these three deformations together. However, our shear zone analysis correlated with the progression in ages and geometry of the intramontane basins show a better separation in three successive, partly overlapping stages where the rotations creates significant strain-partitioning between strike-slip and extension.

4.3. Late miocene upper getic thrusting

The last deformation event observed in our studied area is the thrusting of the Upper Getic sub-unit, which took place likely by reactivating the orogen-perpendicular normal fault system inherited from the Oligocene - early Miocene deformation stage. The age of this event is constrained by the thrusted late Oligocene–early Miocene sediments of the Senje–Resava basin. Field kinematics and regional structures formed during this event truncate all previous ones, while the main thrust is covered by the upper part of Žagubica and Sokobanja Basins sedimentation, which is latest Miocene–Pliocene in age (Fig. 10). Therefore, the age of this top-E thrusting of the Upper Getic sub-unit is late Miocene.

In the northern part of the studied area, the Upper Getic sub-unit is narrow, while thrusting offset is in the order of 1 km (Figs. 4a, b, 10). Here, this unit formed as a fontal trailing imbricated fan of the Supragetic thrust where a possible Cretaceous offset cannot be clearly discriminated from the late Miocene one. Southwards in the studied area, the total offset of the Upper Getic thrust gradually increases to more than 6 km (Fig. 4c–e). This Miocene thrusting forms a large ramp-anticline over the Oligocene–early Miocene sediments of the Senje–Resava Basin (Fig. 4c–e). More southwards, the offset along the Upper Getic thrust decreases rapidly towards the Sokobanja Basin, where this thrust is buried beneath younger sediments (Fig. 10). South of this basin and outside the study area, there is no equivalent of the Upper Getic thrust that can be observed at map scale (Fig. 2). The significant

variability in thrusting along the Upper Getic strike also explains the formation of numerous *E*-W oriented strike-slip tear faults that laterally offset this structure (Fig. 10). Many of these tear faults are in fact lateral ramps that formed as normal faults during the orogen-parallel deformation stage (Fig. 12). These *E*-W normal faults have initially segmented the margin of the Senje–Resava Basin, preserving the late Oligocene-early Miocene sediments in their hanging walls. The lateral variability between late Oligocene-early Miocene sediments and Cretaceous limestones has created a rheologically heterogeneous footwall for the thrusting of the Upper Getic sub-unit (Fig. 12). The large scale tearing and the surface expression of the Upper Getic sub-unit demonstrate the thrusting was controlled by the inherited normal faulting associated with the formation of the Senje–Resava Basin.

5. Discussion

The Cretaceous thrusting of the Supragetic Unit is in agreement with the timing and geometry of the Sasca–Gornjac and Resita nappes defined northwards in the South Carpathians of Romania, emplaced during late Early Cretaceous times in the footwall of the main Supragetic thrust (e.g., Iancu et al., 2005a; Kräutner and Krstić, 2002; Săndulescu, 1984). However, no late Miocene thrusting of the equivalent Upper Getic thrust contact has been observed in the South Carpathians, which is in agreement with our interpretation that the late Miocene reactivation is reducing gradually its offset to zero northwards. It is likely that the Supragetic thrusting took place during the late Early Cretaceous, as observed in the South Carpathians (Fig. 13a). There are no indications that the latest Cretaceous Getic thrusting and the formation of the Danubian nappe stack (Fig. 13a) has also re-activated the Supragetic thrust only in the Serbian Carpathians prior to the subsequent activation of the CernTimok Fault system. However, we cannot completely exclude such a hypothesis due to the lack of further timing indicators, such as thermochronology or post-tectonic covers.

The orogen-perpendicular extension, strike-slip and orogen-parallel extension can be correlated with the formation of Oligocene-Neogene basins. The ~29–27 Ma onset observed in the Jastrebac area (Erak et al., 2017) is the earliest possible age of the orogen-perpendicular extension (Fig. 13b). An orogen-perpendicular back-arc extension driven by the roll-back of a Carpathians slab roll-back is not possible in the N-S Serbian segment adjacent to the fixed Moesian Platform (Fig. 1, see also Matenco and Radivojević, 2012). Therefore, the observed orogen-perpendicular extension must be related to processes active during the evolution of a Dinarides slab, such as slab-detachment or subsequent eduction (Andrić et al., 2018), which is compatible with the observed directions of extension (Figs. 1 and 13b).

5.1. Mechanisms of backarc-convex oroclinal bending

Our kinematic analysis correlated with paleomagnetic rotations measured in the South Carpathians indicate that ~40° of clockwise rotations took place during late Oligocene–middle Miocene times. The kinematics and timing are in agreement with the geometry and moments of activation of the large offset and curved late Oligocene Cerna and early Miocene Timok faults (Figs. 2 and 13b, e.g., Maţenco, 2017; Schmid et al., 2008). This kinematics indicates that oroclinal bending in the Serbian Carpathians has started with strike-slip deformation, which was gradually replaced in the later stages by orogen-parallel extension (Fig. 13b). This overall mechanism is only partly compatible with observations by previous studies in the South Carpathians, where a longer and a more continuous coexistence of strike-slip and orogen-parallel extension has been inferred (Krézsek et al., 2013; Fügenschuh and Schmid, 2005; Matenco and Schmid, 1999). There, oroclinal bending triggered the formation of the Danubian detachment during the Paleocene-Eocene, which remained active until the early middle Miocene, overlapping in time with the activity of Cerna and Timok dextral strike-slip faults and the transtensional formation of the Getic Depression Basin (e.g., Dupont-Nivet et al., 2005; Fügenschuh and Schmid, 2005; Matenco and Schmid, 1999; Moser et al., 2005; Schmid et al., 1998). This basin was subsequently transpressionally inverted in middle-late Miocene times to form the South Carpathians foredeep (e.g., Matenco et al., 2003; Răbăgia et al., 2011). Furthermore, coeval transtension and orogen parallel extension in the South Carpathians has accommodated the observed shortening of the East Carpathians at their contact with the Moesian Platform by a gradual progression of deformation NE- and E- wards during Oligocene–middle Miocene times (Krézsek et al., 2013). In other words, while deformation started with orogen-parallel extension during Paleocene-Eocene and continued with coeval late Oligocene–middle Miocene strike-slip and orogen-parallel extension in the South Carpathians, the studied segment of the Serbian Carpathians indicates a progression from strike-slip to orogen-parallel extension during the latest Oligocene - middle Miocene.

Our studied case of the Serbian Carpathians is the one of a major intra-continental strike-slip fault system (i.e. Cerna–Timok) that formed coevally with oroclinal bending. Although deformation is distributed along a large number of small structures, we observe that oroclinal bending may be also associated with an orogen-perpendicular extension

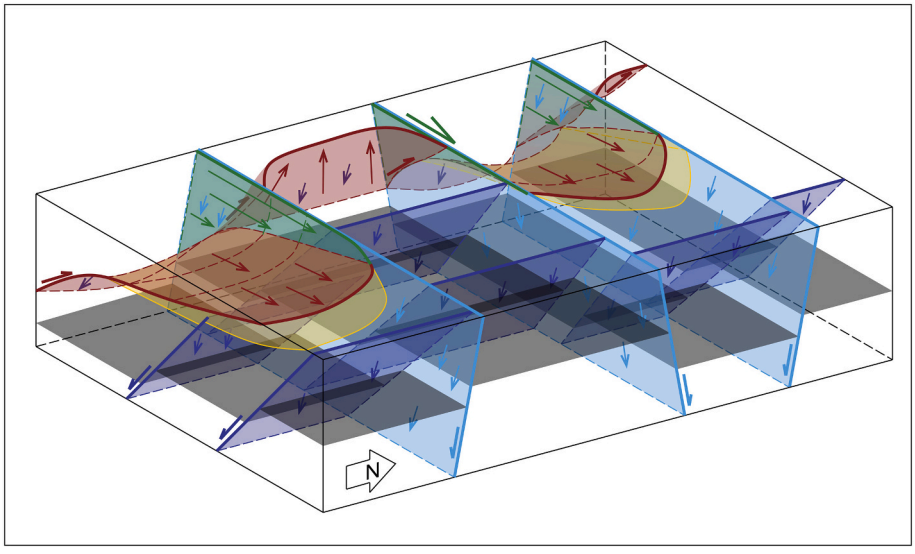

Fig. 12. 3D sketch of structural superposition and mechanics of Oligocene-Miocene extension and subsequent shortening in the vicinity of the Upper Getic thrust. Dark blue normal faults formed during orogen-perpendicular extension, light blue normal faults formed during orogen-parallel extension. These faults control the subsequent formation of thrusts (red) and strike-slip tear faults (green). Sediments of the Senje-Resava Basin are shown in yellow colour, while black horizons are drawn to illustrate offsets along normal faults. Arrows and half arrows show the relative movement of the hanging wall. When faults are re-activated, longer arrows indicate younger movement. (For interpretation of the references to colour in this figure legend, the reader is referred to the web version of this article.)

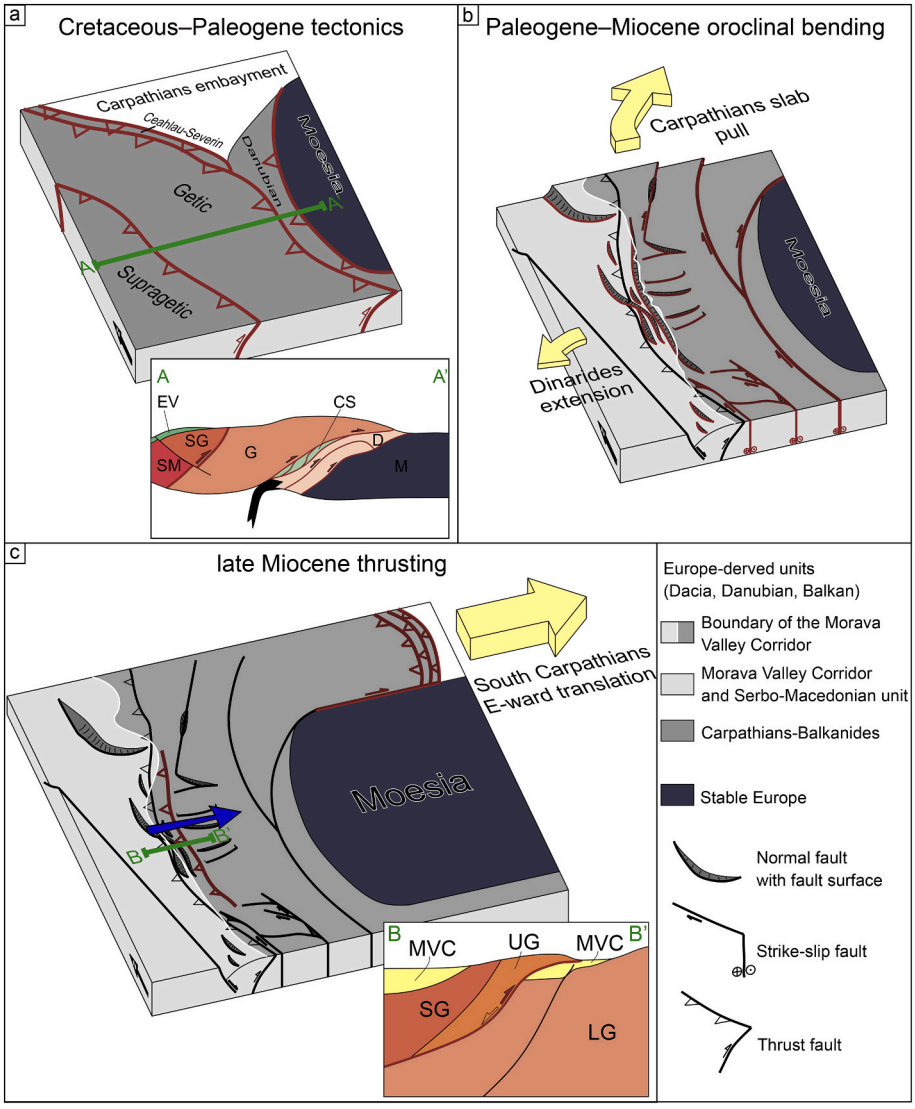

Fig. 13. a) 3D and cross-section sketches of main tectonic units and structures active during the Cretaceous–Paleogene shortening. EV-Eastern Vardar Ophiolitic unit, SM-Serbo-Macedonian unit, SG-Supragetic unit, UG-Upper Getic sub-unit, LG-Lower Getic sub-unit, CS-Ceahlău-Severin unit, D-Danubian units, M-Moesian Platform. 3D sketch is built after map view sketch of Fügenschuh and Schmid (2005). Position of the cross-section is indicated by the green line. b) 3D sketch of oroclinal bending mechanics with complex fault pattern that includes regional dextral strike-slip and orogen-parallel and perpendicular normal faults, mainly controlled by Carpathian slab retreat to the north and north-east, the position of the rigid Moesian indenter and extension in the Dinarides to the west. c) 3D and cross-section sketches of the late Miocene reactivation of the Upper Getic thrust during the indentation by Moesian Platform (stable Europe). Direction of shortening in the Serbian Carpathians is indicated by the blue arrow. Cross-section sketch shows the Upper Getic thrusting over sediments of the Cenozoic basins. Position of the cross-section is indicated by the green line. MVC- Morava Valley Corridor sediments, SG-Supragetic unit, UG-Upper Getic sub-unit, LG-Lower Getic sub-unit. (For interpretation of the references to colour in this figure legend, the reader is referred to the web version of this article.)

that evolves independently from the coupled strike-slip and orogen-parallel deformation. The former is driven by the interference with the geodynamic evolution of a different orogen (i.e. Dinarides). The latter is driven by the orogenic pull exerted by a slab-retreat in a curved orogen, where orogen-parallel deformation starts closer to the slab (i.e., the South Carpathians) and develops progressively at farther distances (i.e., the Serbian Carpathians) in an orogen that gradually reorients itself perpendicular to the trench (i.e., the East Carpathians, Fig. 1).

Such observations are also known from other large-scale continental strike-slip faults, such as San Andreas fault, Alpine fault or Dead Sea fault, which show distributed deformation and strain partitioning in up to hundreds of kilometres wide zones (e.g., Dooley and Schreurs, 2012). Strike-slip shear zones often display oblique movements that create transpressive and/or transtensive deformation forming positive or negative flower structures, transpressional orogens and basins with highly variable geometries (Christie-Blick and Biddle, 1985; Dewey et al., 1998; Dooley and Schreurs, 2012; Leever et al., 2011; Smit et al., 2008, 2010). Furthermore, oblique or curved strike-slip zones show variable amounts of strain partitioning at releasing or restraining bends that show progressive evolution over time (e.g., Dewey et al., 1998; Fossen and Tikoff, 1998; Leever et al., 2011), associated with partitioning in normal or reverse faulting coeval with oroclinal bending (Allen et al., 2003; Hollingsworth et al., 2010; Mattei et al., 2017).

Foreland-convex oroclines dominate the Mediterranean region (Fig. 1a, e.g., Rosenbaum, 2014, and references therein) and are controlled by the retreat of subducting slabs (e.g., Faccenna et al., 2004; Jolivet et al., 2013; Johnston and Mazzoli, 2009; Lonergan and White, 1997). In our studied case of the Serbian Carpathians, the orogen-parallel extension took place during the formation of a back-arc-convex orocline (Fig. 1a and 13b). Such orogen-parallel extension has been observed or inferred during the formation of other backarc-convex oroclines, such as the Cantabrian arc of Ibero-Armorican orogen or Mongolian orocline (e.g., Pastor-Galán et al., 2012, 2015; Ries and Shackleton, 1976; Xiao et al., 2018). The formation of other backarc-convex oroclines has been controlled by orogen-parallel compression induced by two converging cratons (e.g., Mongolian and Kazakhstan oroclines; Edel et al., 2014; Li et al., 2018), collision between two or more rigid blocks with irregular margins (e.g., Alborz Mts., Brasília belt, central Pontides; D'el-Rey Silva et al., 2011; Mattei et al., 2017; Meijers et al., 2010) or the inherited initial curvature of the continental margin of the overriding plate (e.g., Bolivian and Cascadian oroclines; Finley et al., 2019; Isacks, 1988; Johnston et al., 2013; Weil and Sussman, 2004). These observations and correlations show that the type of orogen-parallel deformation is not relevant for the formation of a backarc-convex orocline. These oroclines are spatially controlled by the presence of a rigid, irregular continental block or craton that acts as an

indenter during rotation. In the case of Serbian Carpathians orocline, the rigid Moesian promontory of the European continent controls the oroclinal geometry.

5.2. Late Miocene indentation of the Moesian Platform

Paleomagnetic studies have demonstrated that the large-scale clockwise rotation of the South and East Carpathians around the Moesian indenter has been achieved mostly until middle Miocene times and average ~ 15° afterwards, with a variability controlled by local rotations created by transpressional strike-slip structures (de Leeuw et al., 2013 and references therein; Lesić et al., 2019). The late Miocene thrusting of the Upper Getic sub-unit observed in the Serbian Carpathians is coeval with the Adriatic indentation active in the Dinarides and, at the same time, is also coeval with the Carpathians docking against the Moesian Platform.

To the south and west, the indentation of the Adriatic promontory in the Dinarides inverted the Pannonian Basin and started during the latest Miocene. The effects of this indentation are more pronounced in the NW near the junction with the Southern Alps and in the SE near the other junction with the Albanides–Hellenides (e.g., Bennett et al., 2008; Pinter et al., 2005; Tomljenović et al., 2008). Close to the studied area, this Pannonian Basin inversion is expressed by E-W oriented thrusts and transpressional structures that recorded uplift in the order of few hundred meters (Matenco and Radivojević, 2012; Toljić et al., 2013). However, the N-S contraction direction of these structures is incompatible with the top-E direction of Upper Getic thrusting.

To the north and east, the dextral transpressional docking of the South Carpathians and the last phase of thin-skinned E-ward thrusting of the East Carpathians took place during late middle–late Miocene times and ceased around 8 Ma, at the same time when the extension in the Pannonian Basin areas located north of the Morava Valley Corridor also ceased (e.g., Balázs et al., 2018; Maţenco, 2017). Because the main extension in the Morava Valley Corridor also ceased during middle Miocene times, it is likely that the late Miocene E-ward movement of the South and East Carpathians until 8 Ma was associated with E-ward thrusting reactivation of inherited normal fault between Upper and Lower Getic sub-units in the, by then, N-S oriented segment of the Serbian Carpathians (Figs. 12 and 13c, see also Ustaszewski et al., 2008 and references therein) during the late Miocene. The dextral movement of the E-W oriented South Carpathians in respect to the stable Moesian Platform was partly taken up by thrusting in the N-S oriented segment of the Serbian Carpathians. Such a mechanism would assume that the amount of thrusting gradually decreases as observed northwards in the Serbian Carpathians, while deformation being at the same time gradually transferred to dextral strike-slip north of the Moesian indenter (Fig. 13c), as observed in the South Carpathians (e.g., Matenco and Schmid, 1999). This mechanism should have been active only during late Miocene times, as the last phase of thin-skinned Pliocene–Quaternary deformation is localized only in the area of the SE Carpathians and was not observed in the intervening South Carpathians (e.g., Leever et al., 2006; Maţenco, 2017).

6. Conclusions

In order to understand the formation and evolution of the 180° of oroclinal bending recorded by SE part of the Carpatho–Balkanides orogen, we have performed a kinematic study in the key area of the western Serbian Carpathians. The results demonstrate that this area was affected by a complex poly-phase kinematic evolution that recorded the geodynamic evolution of both the Carpathians and Dinarides orogen.

Following earlier Paleozoic and older deformation, the first shortening event that affected the studied part of the Serbian Carpathians was recorded by the late Early Cretaceous Supragetic thrusting, which is a peak deformation moment recorded during the subduction of the Ceahlău –Severin Ocean and Carpathians continental collision. This thrusting largely pre-dates the oroclinal bending observed in the Serbian Carpathians.

Although not directly prominent in the large-scale orogenic structure, the second deformation event observed in the studied area was associated with a complex strain partitioning between partly overlapping stages of orogen-perpendicular extension, strike-slip and orogen parallel extension. This event took place mostly during the ~40° of oroclinal bending recorded by the studied segment of the Serbian Carpathians, derived from the variability of kinematic directions along the orogenic strike. The orogen-perpendicular extension is also compatible with the Oligocene onset of extension in the Morava Valley Corridor that is likely driven by the slab-detachment and eduction in the Dinarides. In contrast, the oroclinal bending in the studied part of the Serbian Carpathians was accommodated also by strike-slip deformation that was later gradually replaced by orogen parallel extension. This mechanism is compatible with the ~100 km of cumulated dextral strike-slip offset recorded along the curved fault geometry of the Cerna and Timok system located east of the studied area. These new insights on the rotational mechanisms of the Serbian Carpathians are somewhat different when compared with the neighbouring South Carpathians, which recorded first orogen-parallel extension followed by coupled strike-slip and orogen-parallel extension during Paleocene–middle Miocene times.

The last stage of deformation observed is the late Miocene thrusting of the Upper Getic sub-unit. Among all potential geodynamic mechanisms responsible for this thrusting, the one of transfer of deformation from dextral strike-slip at the northern margin of Moesian Platform in the South Carpathians to thrusting at the western margin of the same Moesian Platform in the Serbian Carpathians seems more likely. This deformation was coeval with the last moments of late Miocene thin-skinned thrusting until 8 Ma in the East and SE Carpathians and coeval extension in the Pannonian Basin.

Our study infers that the type of orogen-parallel deformation is not relevant for the formation of a backarc-convex orocline, such as the studied case of the Serbian Carpathians. These oroclines are spatially controlled by the presence of a rigid, irregular continental block or craton that acts like an indenter during rotation. In the case of Serbian Carpathians orocline, the rigid Moesian promontory of the European continent controls the oroclinal geometry. The study also shows the importance of a step-wise kinematic approach to reconstruct the tectonic evolution of highly curved orogens, such as the Carpathians–Balkanides, where strain partitioning is not apparent in their large-scale structure. Such reconstructions based on structural evidence must consider that strain partitioning overprints the inherited orogenic structure, in particular when differential rotations and translations are coeval. Understanding such structures must go beyond standard paleostress studies and must involve strain or shear-zone analysis and independent constraints, such as the coeval evolution of sedimentary basins.

Declaration of Competing Interest

The authors declare that they have no known competing financial interests or personal relationships that could have appeared to influence the work reported in this paper.

Acknowledgements

This paper is part of a collaboration between the Department of Earth Sciences at Utrecht University, the Netherlands and Faculty of Mining and Geology, University of Belgrade, Serbia during the PhD of Nemanja Krstekanić and is funded by the Netherlands Research Centre for Integrated Solid Earth Science (ISES) and the Ministry of Education, Science and Technological Development of the Republic of Serbia, Projects No. OI176015 and OI176019. We would like to thank Miloš Radonjić and Nenad Čokulov for their help during the fieldwork. Employees of PZP Požarevac are thanked for their hospitality during the fieldwork in the

Kaona quarry. Detailed comments of Daniel Pastor-Galán on an earlier manuscript version are gratefully acknowledged. We thank the Editor, Zhengtang Guo and two anonymous reviewers for their detailed comments and suggestions which have significantly improved the original version of manuscript.

Data availability

Measurements, kinematic and structural data obtained in this study are available in Figs. 5–11. The full dataset measured in the field is available in the Supplementary Appendix B.

Appendix A. Supplementary data

Supplementary data to this article can be found online at https://doi.org/10.1016/j.gloplacha.2020.103361.

References

Allen, M.B., Ghassemi, M.R., Shahrabi, M., Qorashi, M., 2003. Accommodation of late Cenozoic oblique shortening in the Alborz range, northern Iran. J. Struct. Geol. 25, 659–672.

Anđelković, J., Krstić, B., Bogdanović, P., Jadranin, D., Milenković, P., Milošaković, R., Urošević, D., Dimitrijević, D., Dolić, D., Rakić, M.O., Jovanović, L.J., Maslarević, L. J., Marković, B., Divljan, M., Đorđević, M., 1977. Explanatory book for sheets Pirot and Breznik, Basic geological map of SFRY 1:100.000. Savezni geološki zavod, Belgrade.

Andrić, N., Sant, K., Matenco, L., Mandic, O., Tomljenović, B., Pavelić, B., Hrvatović, H., Demir, V., Ooms, J., 2017. The link between tectonics and sedimentation in asymmetric extensional basins: inferences from the study of the Sarajevo–Zenica Basin. Mar. Pet. Geol. 83, 305–332.

Andrić, N., Vogt, K., Matenco, L., Cvetković, V., Cloetingh, S., Gerya, T., 2018. Variability of orogenic magmatism during Mediterranean-style continental collisions: a numerical modelling approach. Gondwana Res. 56, 119–134.

Angelier, J., 1994. Fault slip analysis and paleostress reconstruction. In: Hancock, P.L. (Ed.), Continental Deformation. Pergamon Press, Oxford, New York, Seoul, Tokyo, pp. 53–100.

Angelier, J., Goguel, J., 1979. Sur une méthode simple de détermination des axes principaux des constraintes pour une population de failles. Comptes rendus de l'Académie des Sciences, sér. D 288, 307–310.

Angelier, J., Mechler, P., 1977. Sur une méthode graphique de recherche des constraintes principales également utilisable en tectonique et en seismoligie: la méthode des dièdres droits. Bulletin de la Société Géologique de France 7 (19), 1309–1318.

Antić, M.D., Kounov, A., Trivić, B., Wetzel, A., Peytcheva, I., von Quadt, A., 2016a. Alpine thermal events in the central Serbo–Macedonian Massif (southeastern Serbia). Int. J. Earth Sci. 105, 1485–1505.

Antić, M., Peytcheva, I., von Quadt, A., Kounov, A., Trivić, B., Serafimovski, T., Tasev, G., Gerdjikov, I., Wetzel, A., 2016b. Pre-Alpine evolution of a segment of the North-Gondwanan margin: geochronological and geochemical evidence from the central Serbo–Macedonian Massif. Gondwana Res. 36, 523–544.

Antonijević, I., Veselinović, M., Đorđević, M., Kalenić, M., Krstić, B., Karajičić, L.J., 1970. Explanatory book for sheet Žagubica, Basic geological map of SFRY 1:100.000. Savezni geološki zavod, Belgrade.

Bada, G., Horváth, F., Dövényi, P., Szafián, P., Windhoffer, G., Cloetingh, S., 2007. Present-day stress field and tectonic inversion in the Pannonian basin. Glob. Planet. Chang. 58, 165–180.

Balázs, A., Matenco, L., Magyar, I., Horváth, F., Cloetingh, S., 2016. The link between tectonics and sedimentation in back-arc basins: new genetic constraints from the analysis of the Pannonian Basin. Tectonics 35, 1526–1559.

Balázs, A., Magyar, I., Matenco, L., Sztanó, O., Tőkés, L., Horváth, F., 2018. Morphology of a large paleo-lake: analysis of compaction in the Miocene–Quaternary Pannonian Basin. Glob. Planet. Chang. 171, 134–147.

Balla, Z., 1987. Tertiary palaeomagnetic data for the Carpatho–Pannonian region in the light of Miocene rotation kinematics. Tectonophysics 139, 67–98.

Benesh, N.P., Plesch, A., Shaw, J.H., 2014. Geometry, kinematics, and displacement characteristics of tear-fault systems: an example from the deep-water Niger Delta. AAPG Bull. 98 (3), 465–482.

Bennett, R.A., Hreinsdóttir, S., Buble, G., Bašić, T., Bačić, Ž., Marjanović, M., Casale, G., Gendaszek, A., Cowan, D., 2008. Eocene to present subduction of southern Adria mantle lithosphere beneath the Dinarides. Geology 36 (1), 3–6.

Berza, T., Drăgănescu, A., 1988. The Cerna–Jiu fault system (South Carpathians, Romania), a major Tertiary transcurrent lineament. DS Inst. Geol. Geofiz. 72–73, 43–57.

Bojar, A.-V., Neubauer, F., Fritz, H., 1998. Cretaceous to Cenozoic thermal evolution of the southwestern South Carpathians: evidence from fission-track thermochronology. Tectonophysics 297, 229–249.

Calignano, E., Sokoutis, D., Willingshofer, E., Brun, J.-P., Gueydan, F., Cloething, S., 2017. Oblique contractional reactivation of inherited heterogeneities: Cause for arcuate orogens. Tectonics 36, 542–558.

Carey, S.W., 1955. The orocline concept in geotectonics. Pap. Proc. R. Soc. Tasmania 89, 255–288.

Carreras, J., Cosgrove, J.W., Druguet, E., 2013. Strain partitioning in banded and/or anisotropic rocks: implications for inferring tectonic regimes. J. Struct. Geol. 50, 7–21.

Célérier, B., Etchecopar, A., Bergerat, F., Vergely, P., Arthaud, F., Laurent, P., 2012. Inferring stress from faulting: from early concepts to inverse methods. Tectonophysics 581, 206–219.

Cembrano, J., González, G., Arancibia, G., Ahumada, I., Olivares, V., Herrera, V., 2005. Fault zone development and strain partitioning in an extensional strike-slip duplex: a case study from the Mesozoic Atacama fault system, Northern Chile. Tectonophysics 400, 105–125.

Christie-Blick, N., Biddle, K.T., 1985. Deformation and basin formation along strike-slip faults. In: Biddle, K.T., Christie-Blick, N. (Eds.), Strike-Slip Deformation, Basin Formation, and Sedimentation. SEPM Spec. Publ. (No. 37). Society of Economic Paleontologists and Mineralogists, Tulsa, OK, pp. 1–34.

Cifelli, F., Mattei, M., Della Seta, M., 2008. Calabrian Arc oroclinal bending: the role of subduction. Tectonics 27, TC5001. https://doi.org/10.1029/2008TC002272.

Csontos, L., 1995. Cenozoic tectonic evolution of the Intra-Carpathian area: a review. Acta Vulcanol. 7, 1–13.

Csontos, L., Vörös, A., 2004. Mesozoic plate tectonic reconstruction of the Carpathian region. Palaeogeogr. Palaeoclimatol. Palaeoecol. 210, 1–56.

Csontos, L., Nagymarosy, A., Horváth, F., Kovác, M., 1992. Tertiary evolution of the Intra-Carpathian area: a model. Tectonophysics 208, 221–241.

Dallmeyer, R.D., Neubauer, F., Handler, R., Fritz, H., Müller, W., Pana, D., Putis, M., 1996. Tectonothermal evolution of the internal Alps and Carpathians: evidence from $^{40}Ar/^{39}Ar$ mineral and whole-rock data. Eclogae Geol. Helv. 89/1, 203–227.

de Bruijn, H., Marković, Z., Wessels, W., Milivojević, M., van de Weerd, A.A., 2018. Rodent faunas from the Paleogene of south-east Serbia. Palaeobiodiversity Palaeoenviron. 98 (3), 441–458.

de Leeuw, A., Filipescu, S., Maţenco, L., Krijgsman, W., Kuiper, K., Stoica, M., 2013. Paleomagnetic and chronostratigraphic constraints on the Middle to late Miocene evolution of the Transylvanian Basin (Romania): implications for Central Paratethys stratigraphy and emplacement of the Tisza–Dacia plate. Glob. Planet. Chang. 103, 82–98.

De Vicente, G., Regas, R., Muñoz-Martín, A., Van Wees, J.D., Casas-Sáinz, A., Sopeña, A., Sánchez-Moya, P., Arche, A., López-Gómez, J., Oláiz, A., Fernandez Lozano, J., 2009. Oblique strain partitioning and transpression on an inverted rift: the Castilian Branch of the Iberian Chain. Tectonophysics 470, 224–242.

D'el-Rey Silva, L.J.H., de Oliveira, Í.L., Pohren, C.B., Tanizaki, M.L.N., Carneiro, R.C., Fernandes, G.L. de F, Aragão, P.E., 2011. Coeval perpendicular shortenings in the Brasília belt: Collision of irregular plate margins leading to oroclinal bending in the Neoproterozoic of Central Brazil. J. S. Am. Earth Sci. 32, 1–13.

Delvaux, D., Sperner, B., 2003. New aspects of tectonic stress inversion with reference to the TENSOR program. In: Nieuwland, D.A. (Ed.), New Insights into Structural Interpretation and Modelling, Special Publications 212. Geological Society, London, pp. 75–100.

Dewey, J.F., Holdsworth, R.E., Strachan, R.A., 1998. Transpression and transtension zones. In: Holdsworth, R.E., Strachan, R.A., Dewey, J.E. (Eds.), Continental Transpressional and Transtensional Tectonics, Special Publications 135. Geological Society, London, pp. 1–14.

Dimitrijević, M.D., 1997. Geology of Yugoslavia. Geological Institute, Belgrade.

Djordjević-Milutinović, D., 2010. An overview of Paleozoic and Mesozoic sites with macroflora in Serbia. Bull. Nat. Hist. Mus. 3, 27–46.

Doblas, M., 1998. Slickenside kinematic indicators. Tectonophysics 295, 187–197.

Dooley, T.P., Schreurs, G., 2012. Analogue modelling of intraplate strike-slip tectonics: a review and new experimental results. Tectonophysics 574–575, 1–71.

Dupont-Nivet, G., Vasiliev, I., Langereis, C.G., Krijgsman, W., Panaiotu, C., 2005. Neogene tectonic evolution of the southern and eastern Carpathians constrained by paleomagnetism. Earth Planet. Sci. Lett. 236, 374–387.

Edel, J.B., Schulmann, K., Hanžl, P., Lexa, O., 2014. Palaeomagnetic and structural constraints on 90° anticlockwise rotation in SW Mongolia during the Permo–Triassic: implications for Altaid oroclinal bending. Preliminary palaeomagnetic results. J. Asian Earth Sci. 94, 157–171.

Erak, D., Matenco, L., Toljić, M., Stojadinović, U., Andriessen, P.A.M., Willingshofer, E., Ducea, M.N., 2017. From nappe stacking to extensional detachments at the contact between the Carpathians and Dinarides – the Jastrebac Mountains of Central Serbia. Tectonophysics 710–711, 162–183.

Faccenna, C., Piromallo, C., Crespo-Blanc, A., Jolivet, L., Rossetti, F., 2004. Lateral slab deformation and the origin of the western Mediterranean arcs. Tectonics 23, TC1012. https://doi.org/10.1029/2002TC001488.

Faccenna, C., Becker, T.W., Auer, L., Billi, A., Boschi, L., Brun, J.P., Capitanio, F.A., Funiciello, F., Horvàth, F., Jolivet, L., Piromallo, C., Royden, L., Rossetti, F., Serpelloni, E., 2014. Mantle dynamics in the Mediterranean. Rev. Geophys. 52, 283–332.

Finley, T., Morell, K., Leonard, L., Regalla, C., Johnston, S.T., Zhang, W., 2019. Ongoing oroclinal bending in the Cascadia forearc and its relation to concave-outboard plate margin geometry. Geology 47, 155–158.

Fitch, T.J., 1972. Plate convergence, transcurrent faults, and internal deformation adjacent to Southeast Asia and the western Pacific. J. Geophys. Res. 77 (23), 4432–4460.

Fodor, L., Bada, G., Csillag, G., Horváth, E., Ruszkiczay-Rüdiger, Z., Palotás, K., Síkhegyi, F., Timár, G., Cloetingh, S., Horváth, F., 2005. An outline of neotectonic structures and morphotectonics of the western and central Pannonian Basin. Tectonophysics 410, 15–41.

Fossen, H., Tikoff, B., 1998. Extended models of transpression and transtension, and application to tectonic settings. In: Holdsworth, R.E., Strachan, R.A., Dewey, J.E. (Eds.), Continental Transpressional and Transtensional Tectonics, Special Publications 135. Geological Society, London, pp. 15–33.
Fossen, H., Tikoff, G., Teyssier, C., 1994. Strain modeling of transpressional and transtensional deformation. Nor. Geol. Tidsskr. 74, 134–145.
Fügenschuh, B., Schmid, S.M., 2005. Age and significance of core complex formation in a very curved orogen: evidence from fission track studies in the South Carpathians (Romania). Tectonophysics 404, 33–53.
Gallhofer, D., von Quadt, A., Peytcheva, I., Schmid, S.M., Heinrich, C.A., 2015. Tectonic, magmatic, and metallogenic evolution of the Late Cretaceous arc in the Carpathian–Balkan orogen. Tectonics 34, 1813–1836.
Glen, J.M.G., 2004. A kinematic model for the southern Alaska orocline based on regional fault patterns. In: Sussman, A.J., Weil, A.B. (Eds.), Orogenic Curvature: Integrating Paleomagnetic and Structural Analyses: Geological Society of America Special Paper 383. Geological Society of America, Boulder, CO, pp. 161–172.
Gutiérrez-Alonso, G., Collins, A.S., Fernández-Suárez, J., Pastor-Galán, D., González-Clavijo, E., Jourdan, F., Weil, A.B., Johnston, S.T., 2015. Dating of lithospheric buckling: $^{40}Ar/^{39}Ar$ ages of syn-orocline strike-slip shear zones in northwestern Iberia. Tectonophysics 643, 44–54.
Hippolyte, J.-C., Bergerat, F., Gordon, M.B., Bellier, O., Espurt, N., 2012. Keys and pitfalls in mesoscale fault analysis and paleostress reconstructions, the use of Angelier's methods. Tectonophysics 581, 144–162.
Hollingsworth, J., Fattahi, M., Walker, R., Talebian, M., Bahroudi, A., Bolourchi, M.J., Jackson, J., Copley, A., 2010. Oroclinal bending, distributed thrust and strike-slip faulting, and the accommodation of Arabia–Eurasia convergence in NE Iran since the Oligocene. Geophys. J. Int. 181, 1214–1246.
Horváth, F., Bada, G., Szafián, P., Tari, G., Ádám, A., Cloetingh, S., 2006. Formation and deformation of the Pannonian Basin: constraints from observational data. Geol. Soc. Lond. Mem. 32, 191–206.
Horváth, F., Musitz, B., Balázs, A., Végh, A., Uhrin, A., Nádor, A., Koroknai, B., Pap, N., Tóth, T., Wórum, G., 2015. Evolution of the Pannonian basin and its geothermal resources. Geothermics 53, 328–352.
Iancu, V., Berza, T., Seghedi, A., Gheuca, I., Hann, H.-P., 2005a. Alpine polyphase tectono-metamorphic evolution of the South Carpathians: a new overview. Tectonophysics 410, 337–365.
Iancu, V., Berza, T., Seghedi, A., Maruntiu, M., 2005b. Paleozoic rock assemblages incorporated in the South Carpathian Alpine thrust belt (Romania and Serbia): a review. Geol. Belg. 8 (4), 48–68.
Isacks, B.L., 1988. Uplift of the Central Andean plateau and bending of the bolivian orocline. J. Geophys. Res. 93, 3211–3231.
Johnston, S.T., Mazzoli, S., 2009. The Calabrian Orocline: buckling of a previously more linear orogen. In: Murphy, J.B., Keppie, J.D., Hynes, A.J. (Eds.), Ancient Orogens and Modern Analogues, Geological Society Special Publications 327. The Geological Society of London, London, pp. 113–125.
Johnston, S.T., Weil, A.B., Gutiérrez-Alonso, G., 2013. Oroclines: thick and thin. GSA Bull. 125 (5/6), 643–663.
Jolivet, L., Faccenna, C., Huet, B., Labrousse, L., Le Pourhiet, L., Lacombe, O., Lecomte, E., Burov, E., Denèle, Y., Brun, J.-P., Philippon, M., Paul, A., Salaün, G., Karabulut, H., Piromallo, C., Monié, P., Gueydan, F., Okay, A.I., Oberhänsli, R., Pourteau, A., Augier, R., Gadenne, L., Driussi, O., 2013. Aegean tectonics: strain localisation, slab tearing and trench retreat. Tectonophysics 597–598, 1–33.
Jones, R.R., Tanner, P.W.G., 1995. Strain partitioning in transpression zones. J. Struct. Geol. 17 (6), 793–802.
Kalenić, M., Hadži-Vuković, M., Dolić, D., Lončarević, Č., Rakić, M.O., 1980. Explanatory book for sheet Kučevo, basic geological map of SFRY 1:100.000. Savezni geološki zavod, Belgrade.
Kolb, M., von Quadt, A., Peytcheva, I., Heinrich, C.A., Fowler, S.J., Cvetković, V., 2013. Adakite-like and normal arc magmas: distinct fractionation paths in the East Serbian Segment of the Balkan–Carpathian Arc. J. Petrol. 54 (3), 421–451.
Kounov, A., Burg, J.-P., Bernoulli, D., Seward, D., Ivanov, Z., Dimov, D., Gerdjikov, I., 2011. Paleostress analysis of Cenozoic faulting in the Kraishte area, SW Bulgaria. J. Struct. Geol. 33, 859–874.
Kräutner, H.G., Krstić, B., 2002. Alpine and Pre-Alpine structural units within Southern Carpathians and the Eastern Balkanides. In: Proceedings of XVII Congress of Carpathian–Balkan Geological Association, Geologica Carpathica, 53 (Special Issue).
Kräutner, H.G., Krstić, B., 2003. Geological Map of the Carpatho–Balkanides between Mehadia, Oravița, Niš and Sofia. Geoinstitute, Belgrade.
Krézsek, C., Lăpădat, A., Maţenco, L., Arnberger, K., Barbu, V., Olaru, R., 2013. Strain partitioning at orogenic contacts during rotation, strike-slip and oblique convergence: Paleogene–early Miocene evolution of the contact between the South Carpathians and Moesia. Glob. Planet. Chang. 103, 63–81.
Krstekanić, N., Stojadinović, U., Kostić, B., Toljić, M., 2017. Internal structure of the Supragetic Unit basement in the Serbian Carpathians and its significance for the late early cretaceous nappe-stacking. Annalés Géologiques de la Péninsule Balkanique 78, 1–15.
Krstić, N., Jovanović, G., Savić, Lj, Bodor, E., 2003. Lower Miocene lakes of the Balkan Land. Acta Geol. Hung. 46 (3), 291–299.
Lacombe, O., 2012. Do fault slip data inversions actually yield "paleostresses" that can be compared with contemporary stresses? A critical discussion. Compt. Rendus Geosci. 344, 159–173.
Lazarević, Z., Milivojević, J., 2010. Early Miocene flora of the intramontane Žagubica Basin (Serbian Carpatho–Balkanides). N. Jb. Geol. Paläont. (Abh.) 256 (2), 141–150.
Leever, K.A., Matenco, L., Bertotti, G., Cloetingh, S., Drijkoningen, G.G., 2006. Late orogenic vertical movements in the Carpathian Bend Zone—seismic constraints on the transition zone from orogen to foredeep. Basin Res. 18 (4), 521–545.
Leever, K.A., Gabrielsen, R.H., Sokoutis, D., Willingshofer, E., 2011. The effect of convergence angle on the kinematic evolution of strain partitioning in transpressional brittle wedges: insight from analog modeling and high-resolution digital image analysis. Tectonics 30, TC2013. https://doi.org/10.1029/2010TC002823.
Lesić, V., Márton, E., Gajić, V., Jovanović, D., Cvetkov, V., 2019. Clockwise vertical-axis rotation in the West Vardar zone of Serbia: tectonic implications. Swiss J. Geosci. 112, 199–215.
Li, P., Rosenbaum, G., 2014. Does the Manning Orocline exist? New structural evidence from the inner hinge of the Manning Orocline (eastern Australia). Gondwana Res. 25, 1599–1613.
Li, P., Sun, M., Rosenbaum, G., Yuan, C., Safonova, I., Cai, K., Jiang, Y., Zhang, Y., 2018. Geometry, kinematics and tectonic models of the Kazakhstan Orocline, Central Asian Orogenic Belt. J. Asian Earth Sci. 153, 42–56.
Lihoreau, F., Blondel, C., Barry, J., Brunet, M., 2004. A new species of the genus *Microbunodon* (Anthracotheriidae, Artiodactyla) from the Miocene of Pakistan: genus revision, phylogenetic relationships and palaeobiogeography. Zool. Scr. 33 (2), 97–115.
Lisle, R.J., 2013. A critical look at the Wallace-Bott hypothesis in fault-slip analysis. Bull. Soc. Géol. France 184 (4–5), 299–306.
Lister, G.S., Williams, P.F., 1983. The partitioning of deformation in flowing rock masses. Tectonophysics 92, 1–33.
Lonergan, L., White, N., 1997. Origin of the Betic-Rif mountain belt. Tectonics 16 (3), 504–522.
Mai, D.H., 1995. Tertiäre Vegetationsgeschichte Europas. Methoden und Ergebnisse. Gustav Fischer Verlag, Jena, Stuttgart, New York.
Maksimović, B.B., 1956. Geological and tectonical relations of the coal bearing formations of the Senjsko–Resavski mines and the surrounding area. In: Special editions of the Geological institute, 6, pp. 1–104. "Jovan Žujević".
Marković, Z., 2003. The Miocene small mammals of Serbia, a review. Deinsea 10, 393–398.
Marković, Z., Wessels, W., van de Weerd, A.A., de Bruijn, H., 2017. On a new diatomyid (Rodentia, Mammalia) from the Paleogene of south-east Serbia, the first record of the family in Europe. Palaeobiodiv. Palaeoenviron. 98 (3), 459–469.
Marović, M., Djoković, I., Milićević, V., Toljić, M., Gerzina, N., 2002. Paleomagnetism of the late Paleogene and Neogene rocks of the Serbian Carpatho–Balkanides: Tectonic implications. Annalés Géologiques de la Péninsule Balkanique 64, 1–12.
Marović, M., Toljić, M., Rundić, Lj, Milivojević, J., 2007. Neoalpine Tectonics of Serbia. Serbian Geological Society, Belgrade.
Martínez-García, P., Comas, M., Soto, J.I., Lonergan, L., Watts, A.B., 2013. Strike-slip tectonics and basin inversion in the Western Mediterranean: the Post-Messinian evolution of the Alboran Sea. Basin Res. 25, 361–387.
Márton, E., 2000. The Tisza megatectonic unit in the light of paleomagnetic data. Acta Geol. Hung. 43 (3), 329–343.
Márton, E., Tischler, M., Csontos, L., Fügenschuh, B., Schmid, S.M., 2007. The contact zone between the ALCAPA and Tisza–Dacia mega-tectonic units of Northern Romania in the light of new paleomagnetic data. Swiss J. Geosci. 100 (1), 109–124.
Maţenco, L., 2017. Tectonics and exhumation of Romanian Carpathians: inferences from kinematic and thermochronological studies. In: Rădoane, M., Vespremeanu-Stroe, A. (Eds.), Landform Dynamics and Evolution in Romania, Springer geography. Springer, pp. 15–56.
Matenco, L., Radivojević, D., 2012. On the formation and evolution of the Pannonian Basin: constraints derived from the structure of the junction area between the Carpathians and Dinarides. Tectonics 31, TC6007. https://doi.org/10.1029/2012TC003206.
Matenco, L., Schmid, S., 1999. Exhumation of the Danubian nappes system (South Carpathians) during the early Tertiary: inferences from kinematic and paleostress analysis at the Getic/Danubian nappes contact. Tectonophysics 314, 401–422.
Matenco, L., Bertotti, G., Cloetingh, S., Dinu, C., 2003. Subsidence analysis and tectonic evolution of the external Carpathian–Moesian Platform region during Neogene times. Sediment. Geol. 156, 71–94.
Mattei, M., Cifelli, F., Alimohammadian, H., Rashid, H., Winkler, A., Sagnotti, L., 2017. Oroclinal bending in the Alborz Mountains (Northern Iran): new constraints on the age of South Caspian subduction and extrusion tectonics. Gondwana Res. 42, 13–28.
Meijers, M.J.M., Kaymakci, N., van Hinsbergen, D.J.J., Langereis, C.G., Stephenson, R.A., Hippolyte, J.-C., 2010. Late Cretaceous to Paleocene oroclinal bending in the central Pontides (Turkey). Tectonics 29, TC4016. https://doi.org/10.1029/2009TC002620.
Menant, A., Jolivet, L., Vrielynck, B., 2016a. Kinematic reconstructions and magmatic evolution illuminating crustal and mantle dynamics of the eastern Mediterranean region since the late Cretaceous. Tectonophysics 675, 103–140.
Menant, A., Sternai, P., Jolivet, L., Guillou-Frottier, L., Gerya, T., 2016b. 3D numerical modeling of mantle flow, crustal dynamics and magma genesis associated with slab roll-back and tearing: the eastern Mediterranean case. Earth Planet. Sci. Lett. 442, 93–107.
Mladenović, A., Trivić, B., Cvetković, V., 2015. How tectonics controlled post-collisional magmatism within the Dinarides: Inferences based on study of tectono-magmatic events in the Kopaonik Mts. (Southern Serbia). Tectonophysics 646, 36–49.
Mladenović, A., Antić, M.D., Trivić, B., Cvetković, V., 2019. Investigating distant effects of the Moesian promontory: brittle tectonics along the western boundary of the Getic unit (East Serbia). Swiss J. Geosci. 112, 143–161.
Mortimer, N., 2014. The oroclinal bend in the South Island, New Zealand. J. Struct. Geol. 64, 32–38.
Moser, F., Hann, H.P., Dunkl, I., Frisch, W., 2005. Exhumation and relief history of the Southern Carpathians (Romania) as evaluated from apatite fission track chronology in crystalline basement and intramontane sedimentary rocks. Int. J. Earth Sci. 94, 218–230.

Neubauer, F., 2015. Cretaceous tectonics in Eastern Alps, Carpathians and Dinarides: two-step microplate collision and Andean-type magmatic arc associated with orogenic collapse. Rend. Online Soc. Geol. It. 37, 40–43.
Neubauer, F., Bojar, A.-V., 2013. Origin of sediments during Cretaceous continent—continent collision in the Romanian Southern Carpathians: preliminary constraints from $^{40}Ar/^{39}Ar$ single-grain dating of detrital white mica. Geol. Carpath. 64 (5), 375–382.
Obradović, J., Vasić, N., 2007. Jezerski baseni u neogenu Srbije. Special Issues, 662. Serbian Academy of Sciences and Arts, Belgrade.
Orife, T., Lisle, R.J., 2003. Numerical processing of palaeostress results. J. Struct. Geol. 25, 949–957.
Pamić, J.J., 1984. Triassic magmatism of the Dinarides in Yugoslavia. Tectonophysics 109, 273–307.
Pamić, J., 2002. The Sava-Vardar Zone of the Dinarides and Hellenides versus the Vardar Ocean. Eclogae Geol. Helv. 95, 99–113.
Panaiotu, C.G., Panaiotu, C.E., 2010. Palaeomagnetism of the Upper Cretaceous Sânpetru Formation (Haţeg Basin, South Carpathians). Palaeogeogr. Palaeoclimatol. Palaeoecol. 293, 343–352.
Pastor-Galán, D., Gutiérrez-Alonso, G., Weil, A.B., 2011. Orocline timing through joint analysis: insights from the Ibero-Armorican Arc. Tectonophysics 507, 31–46.
Pastor-Galán, D., Gutiérrez-Alonso, G., Zulauf, G., Zanella, F., 2012. Analogue modeling of lithospheric-scale orocline buckling: constraints on the evolution of the Iberian-Armorican Arc. GSA Bull. 124 (7–8), 1293–1309.
Pastor-Galán, D., Ursem, B., Meere, P., Lanereis, C.G., 2015. Extending the Cantabrian Orocline to two continents (Gondwana and Laurussia). Paleomagnetism from South Ireland. Earth Planet. Sci. Lett. 432, 223–231.
Pătrașcu, S., Bleahu, M., Panaiotu, C., 1990. Tectonic implications of paleomagnetic research into upper cretaceous magmatic rocks in the Apuseni Mountains, Romania. Tectonophysics 180, 309–322.
Pătrașcu, S., Bleahu, M., Panaiotu, C., Panaiotu, C.E., 1992. The paleomagnetism of the Upper cretaceous magmatic rocks in the Banat area of the South Carpathians: tectonic implications. Tectonophysics 213, 341–352.
Pătrașcu, S., Şeclăman, M., Panaiotu, C., 1993. Tectonic implications of paleomagnetism in upper cretaceous deposits in the Haţeg and Rusca Montană basins (South Carpathians, Romania). Cretac. Res. 14, 255–264.
Pătrașcu, S., Panaiotu, C., Şeclăman, M., Panaiotu, C.E., 1994. Timing of rotational motion of Apuseni Mountains (Romania): paleomagnetic data from Tertiary magmatic rocks. Tectonophysics 233, 163–176.
Pavlović, M.B., 1997. *Anthracotherium* iz Bogovine (istočna Srbija). Annalés Géologiques de la Péninsule Balkanique 61, 153–160.
Petković, K. (Ed.), 1975. Geologija Srbije: Stratigrafija – prekambrijum i paleozoik. Faculty of Mining and Geology, Belgrade.
Pinter, N., Grenerczy, G., Weber, J., Stein, S., Medak, D. (Eds.), 2005. The Adria Microplate: GPS Geodesy, Tectonics and Hazards (Nato Science Series: IV: Earth and Environmental Sciences). Springer, Dodrecht, the Netherlands.
Platt, J.P., 1993. Mechanics of oblique convergence. J. Geophys. Res. 98 (B9), 16239–16256.
Platt, J.P., Allerton, S., Kirker, A., Mandeville, C., Mayfield, A., Platzman, E.S., Rimi, A., 2003. The ultimate arc: differential displacement, oroclinal bending, and vertical axis rotation in the External Betic-Rif arc. Tectonics 22/3, 1017. https://doi.org/10.1029/2001TC001321.
Porkoláb, K., Kövér, S., Benkó, Z., Héja, G.H., Fialowski, M., Soós, B., Gerzina Spajić, N., Đerić, N., Fodor, L., 2019. Structural and geochronological constraints from the Drina-Ivanjica thrust sheet (Western Serbia): implications for the Cretaceous–Paleogene tectonics of the Internal Dinarides. Swiss J. Geosci. 112, 217–234.
Răbăgia, T., Matenco, L., Cloetingh, S., 2011. The interplay between eustacy, tectonics and surface processes during the growth of a fault-related structure as derived from sequence stratigraphy: the Govora–Ocnele Mari antiform, South Carpathians. Tectonophysics 502, 196–220.
Ratschbacher, L., Linzer, H.G., Moser, F., Strusievicz, R.O., Bedelean, H., Har, N., Mogos, P.A., 1993. Cretaceous to Miocene thrusting and wrenching along the central South Carpathians due to a corner effect during collision and orocline formation. Tectonics 12, 855–873.
Ries, A.C., Shackleton, R.M., 1976. Patterns of strain variation in arcuate fold belts. Philos. Trans. R. Soc. Lond. A 283, 281–288.
Roldán, F.J., Galindo-Zaldívar, J., Ruano, P., Chalouan, A., Pedrera, A., Ahmamou, M., Ruiz-Costán, A., Sanz de Galdeano, C., Benmakhlouf, M., López-Garrido, A.C., Anahnah, F., González-Castillo, L., 2014. Basin evolution associated to curved thrusts: the Prerif Ridges in the Volubilis area (Rif Cordillera, Morocco). J. Geodyn. 77, 56–69.
Rosenbaum, G., 2012. Oroclines of the southern New England Orogen, eastern Australia. Episodes 35 (1), 187–194.
Rosenbaum, G., 2014. Geodynamics of oroclinal bending: Insights from the Mediterranean. J. Geodyn. 82, 5–15.
Săndulescu, M. (Ed.), 1984. Geotectonica României (Translated Title: Geotectonics of Romania). Tehnică, Bucharest.
Săndulescu, M., 1988. Cenozoic tectonic history of the carpathians. In: Royden, L.H., Horvath, F. (Eds.), The Pannonian basin, a study in basin evolution, AAPG Memoir, 45. American Association of Petroleum Geologists, Tulsa, OK, pp. 17–25.
Sant, K., Mandic, O., Rundić, Lj, Kuiper, K.F., Krijgsman, W., 2018. Age and evolution of the Serbian Lake System: integrated results from Middle Miocene Lake Popovac. Newsl. Stratigr. 51 (1), 117–143.
Schefer, S.C., 2012. Tectono-Metamorphic and Magmatic Evolution of the Internal Dinarides (Kopaonik area, southern Serbia) and Its Significance for the Geodynamic Evolution of the Balkan Peninsula (Doctoral dissertation). Retrieved from edoc (http://edoc.unibas.ch/diss/DissB_9908). University of Basel, Basel, Switzerland.
Schmid, S.M., Berza, T., Diaconescu, V., Froitzheim, N., Fügenschuh, B., 1998. Orogen-parallel extension in the Southern Carpathians. Tectonophysics 297, 209–228.
Schmid, S.M., Bernoulli, D., Fügenschuh, B., Matenco, L., Schefer, S., Schuster, R., Tischler, M., Ustaszewski, K., 2008. The Alpine–Carpathian–Dinaridic orogenic system: correlation and evolution of tectonic units. Swiss J. Geosci. 101, 139–183.
Schmid, S.M., Fügenschuh, B., Kounov, A., Matenco, L., Nievergelt, P., Oberhänsli, R., Pleuger, J., Schefer, S., Schuster, R., Tomljenović, B., Ustaszewski, K., van Hinsbergen, D.J.J., 2020. Tectonic units of the Alpine collision zone between Eastern Alps and western Turkey. Gondwana Res. 78, 308–374.
Seghedi, A., Berza, T., Iancu, V., Mărunţiu, M., Oaie, G., 2005. Neoproterozoic terranes in the Moesian basement and in the Alpine Danubian nappes of the South Carpathians. Geol. Belg. 8 (4), 4–19.
Simpson, C., Schmid, S.M., 1983. An evaluation of criteria to deduce the sense of movement in sheared rocks. Geol. Soc. Am. Bull. 94, 1281–1288.
Smit, J., Brun, J.-P., Cloetingh, S., Ben-Avraham, Z., 2008. Pull-apart basin formation and development in narrow transform zones with application to the Dead Sea Basin. Tectonics 27, TC6018. https://doi.org/10.1029/2007TC002119.
Smit, J., Brun, J.-P., Cloetingh, S., Ben-Avraham, Z., 2010. The rift-like structure and asymmetry of the Dead Sea Fault. Earth Planet. Sci. Lett. 290, 74–82.
Sperner, B., Zweigel, P., 2010. A plea for more cauton in fault-slip analysis. Tectonophysics 482, 29–41.
Stampfli, G.M., Borel, G.D., 2002. A plate tectonic model for the Paleozoic and Mesozoic constrained by dynamic plate boundaries and restored synthetic oceanic isochrons. Earth Planet. Sci. Lett. 196, 17–33.
Stojadinovic, U., Matenco, L., Andriessen, P.A.M., Toljić, M., Foeken, J.P.T., 2013. The balance between orogenic building and subsequent extension during the Tertiary evolution of the NE Dinarides: Constraints from low-temperature thermochronology. Glob. Planet. Chang. 103, 19–38.
Stojadinovic, U., Matenco, L., Andriessen, P., Toljić, M., Rundić, Lj, Ducea, M.N., 2017. Structure and provenance of Late Cretaceous–Miocene sediments located near the NE Dinarides margin: Inferences from kinematics of orogenic building and subsequent extensional collapse. Tectonophysics 710–711, 184–204.
ter Borgh, M., Vasiliev, I., Stoica, M., Knežević, S., Matenco, L., Krijgsman, W., Rundić, Lj, Cloetingh, S., 2013. The isolation of the Pannonian basin (Central Paratethys): new constraints from magnetostratigraphy and biostratigraphy. Glob. Planet. Chang. 103, 99–118.
Tikoff, B., Wojtal, S.F., 1999. Displacement control of geologic structures. J. Struct. Geol. 21, 959–967.
Toljić, M., Matenco, L., Ducea, M.N., Stojadinović, U., Milivojević, J., Đerić, N., 2013. The evolution of a key segment in the Europe–Adria collision: the Fruška Gora of northern Serbia. Glob. Planet. Chang. 103, 39–62.
Toljić, M., Matenco, L., Stojadinović, U., Willingshofer, E., Ljubović-Obradović, D., 2018. Understanding fossil fore-arc basins: Inferences from the Cretaceous Adria-Europe convergence in the NE Dinarides. Glob. Planet. Chang. 171, 167–184.
Tomljenović, B., Csontos, L., Márton, E., Márton, P., 2008. Tectonic evolution of the northwestern Internal Dinarides as constrained by structures and rotation of Medvednica Mountains, North Croatia. In: Siegesmund, S., Fügenschuh, B., Froitzheim, N. (Eds.), Tectonic Aspects of the Alpine–Dinaride–Carpathian System. Special Publications. Geological Society, London, pp. 145–167.
Torres Carbonell, P.J., Guzmán, C., Yagupsky, D., Dimieri, L.V., 2016. Tectonic models for the Patagonian orogenic curve (southernmost Andes): an appraisal based on analog experiments from the Fuegian thrust–fold belt. Tectonophysics 671, 76–94.
Ustaszewski, K., Schmid, S.M., Fügenschuh, B., Tischler, M., Kissling, E., Spakman, W., 2008. A map-view restoration of the Alpine–Carpathian–Dinaridic system for the early Miocene. Swiss J. Geosci. 101, 273–294.
Ustaszewski, K., Schmid, S.M., Lugović, B., Schuster, R., Schaltegger, U., Bernoulli, D., Hottinger, L., Kounov, A., Fügenschuh, B., Schefer, S., 2009. Late cretaceous intra-oceanic magmatism in the internal Dinarides (northern Bosnia and Herzegovina): Implications for the collision of the Adriatic and European plates. Lithos 108, 106–125.
Ustaszewski, K., Kounov, A., Schmid, S.M., Schaltegger, U., Krenn, E., Frank, W., Fügenschuh, B., 2010. Evolution of the Adria-Europe plate boundary in the northern Dinarides: from continent-continent collision to back-arc extension. Tectonics 29, TC6017. https://doi.org/10.1029/2010TC002668.
van Hinsbergen, D.J.J., Dupont-Nivet, G., Nakov, R., Oud, K., Panaiotu, C., 2008. No significant post-Eocene rotation of the Moesian Platform and Rhodope (Bulgaria): implications for the kinematic evolution of the Carpathian and Aegean arcs. Earth Planet. Sci. Lett. 273, 345–358.
van Hinsbergen, D.J.J., Torsvik, T.H., Schmid, S.M., Maţenco, L.C., Maffione, M., Vissers, R.L.M., Gürer, D., Spakman, W., 2020. Orogenic architecture of the Mediterranean region and kinematic reconstruction of its tectonic evolution since the Triassic. Gondwana Res. 81, 79–229.
Vergés, J., Fernàndez, M., 2012. Tethys–Atlantic interaction along the Iberia–Africa plate boundary: the Betic–Rif orogenic system. Tectonophysics 579, 144–172.
Veselinović, M., Antonijević, I., Milošaković, R., Mićić, I., Krstić, B., Čićulić, M., Divljan, M., Maslarević, L.J., 1970. Explanatory book for sheet Boljevac, Basic geological map of SFRY 1:100.000. Savezni geološki zavod, Belgrade.
Visarion, M., Săndulescu, M., Stănică, D., Veliciu, S., 1988. Contributions á la connaissance de la structure profonde de la plate-forme Moésienne en Roumanie. St. Tehn. Econ. Geofiz. 15, 68–92.
von Quadt, A., Moritz, R., Peytcheva, I., Heinrich, C.A., 2005. 3:Geochronology and geodynamics of Late Cretaceous magmatism and Cu-Au mineralization in the Panagyurishte region of the Apuseni–Banat–Timok–Srednogorie belt, Bulgaria. Ore Geol. Rev. 27, 95–126.

Vujisić, T., Navala, M., Kalenić, M., Krstić, B., Maslarević, L.J., Marković, B., Buković, J., 1980. Explanatory book for sheet Bela Palanka, Basic geological map of SFRY 1: 100.000. Savezni geološki zavod, Belgrade.
Vujisić, T., Kalenić, M., Navala, M., Lončarević, Č., 1981. Explanatory book for sheet Lapovo, basic geological map of SFRY 1:100.000. Savezni geološki zavod, Belgrade.
Weil, A.B., Sussman, A.J., Sussman, A.J., Weil, A.B., 2004. Classifying curved orogens based on timing relationships between structural development and vertical-axis rotations. In: Orogenic Curvature: Integrating Paleomagnetic and Structural Analysis: Geological Society of America Special Paper, 383, pp. 1–15.
Willingshofer, E., Neubauer, F., Cloetingh, S., 1999. The significance of Gosau–Type Basins for the Late Cretaceous Tectonic history of the Alpine–Carpathian Belt. Phys. Chem. Earth (A) 24 (8), 687–695.
Xiao, W., Windley, B.F., Han, C., Liu, W., Wan, B., Zhang, J., Ao, S., Zhang, Z., Song, D., 2018. Late Paleozoic to early Triassic multiple roll-back and oroclinal bending of the Mongolia collage in Central Asia. Earth Sci. Rev. 186, 94–128.
Žujović, J.M., 1886. Geologische Uebersicht des Königreiches Serbien. Jahrb. Geol. Bundesanst. 36, 71–126.
Zweigel, P., Ratschbacher, L., Frisch, W., 1998. Kinematics of an arcuate fold-thrust belt: the southern Eastern Carpathians (Romania). Tectonophysics 297, 177–207.